

1 An Evaluation of the Performance of Sea-Bird Scientific's Autonomous SeaFET™:  
2 Considerations for the Broader Oceanographic Community

3  
4 Cale A. Miller<sup>1,3</sup>, Katie Pocock<sup>2</sup>, Wiley Evans<sup>2</sup>, and Amanda L. Kelley<sup>1\*</sup>

5  
6 1. College of Fisheries and Ocean Sciences, University of Alaska Fairbanks, Fairbanks, AK,  
7 USA

8  
9 2. Hakai Institute, Heriot Bay, BC, Canada

10  
11 3. **Present address:** Department of Evolution and Ecology, College of Biological Sciences,  
12 University of California Davis, CA, USA

13  
14 \*Correspondence to: Amanda L. Kelley (alkelley@alaska.edu)

15  
16  
17 **Abstract**

18  
19 The commercially available Sea-Bird SeaFET™ provides an accessible way for a broad  
20 community of researchers to study ocean acidification and obtain robust measurements of  
21 seawater pH via the use of an *in situ* autonomous sensor. There are pitfalls, however, that have  
22 been detailed in previous best practices for sensor care, deployment, and data handling. Here, we  
23 took advantage of two distinctly different coastal settings to evaluate the Sea-Bird SeaFET™ and  
24 examine the multitude of scenarios in which problems may arise confounding the accuracy of  
25 measured pH. High-resolution temporal measurements of pH were obtained during 3- to 5-month  
26 field deployments in three separate locations (two in south-central, Alaska, USA, and one British  
27 Columbia, Canada) spanning a broad range of nearshore temperature and salinity conditions.  
28 Both the internal and external electrodes onboard the SeaFET™ were evaluated against robust  
29 benchtop measurements for accuracy utilizing either the factory calibration, an *in situ* single-  
30 point calibration, or *in situ* multi-point calibration. In addition, two sensors deployed in parallel  
31 in Kasitsna Bay, AK, USA, were compared for inter-sensor variability in order to quantify other  
32 factors contributing to SeaFET™ intrinsic inaccuracies. Based on our results, the multi-point  
33 calibration method provided the highest accuracy (< 0.025 difference in pH) of pH when  
34 compared against benchtop measurements. Spectral analysis of time series data showed that  
35 during spring in Alaskan waters, a range of tidal frequencies dominated pH variability, while  
36 seasonal oceanographic conditions were the dominant driver in Canadian waters. Further, it is  
37 suggested that spectral analysis performed on initial deployments may be able to act as an *a*  
38 *posteriori* method to better identify appropriate calibration regimes. Based on this evaluation, we  
39 provide a comprehensive assessment of the potential sources of uncertainty associated with  
40 accuracy and precision of the SeaFETs™ electrodes.

41  
42 **1 Introduction**

43  
44 The intrusion of excess anthropogenic CO<sub>2</sub> into the global oceans—referred to as ocean  
45 acidification (OA)—induces a series of geochemical reactions that increases seawater [H<sup>+</sup>]  
46 (lowering pH) while concomitantly reducing the ocean's overall buffering capacity by reducing

47 the  $[\text{CO}_3^{2-}]$  (Caldeira and Wickett, 2003; Orr et al., 2005). Due to more dynamic natural physical  
48 and chemical processes in the coastal ocean, a differentiation exists between open-ocean  
49 acidification and nearshore coastal acidification. Open-ocean acidification of surface waters is  
50 predominately a function of equilibration with atmospheric  $p\text{CO}_2$ , thus increasing on yearly and  
51 decadal timescales as continued burning of fossil fuels ensues (Hofmann et al., 2011; Orr et al.,  
52 2005). Coastal acidification, however, can manifest on short time and space scales driven by  
53 riverine input and its chemical constituents (e.g., organic carbon, nutrients, and organic  
54 alkalinity), community metabolism and organization, tidal cycles, upwelling, and groundwater  
55 input (Duarte et al., 2013; Sunda and Cai, 2012; Waldbusser and Salisbury, 2014), all of which  
56 can act in conjunction with increasing atmospheric  $\text{CO}_2$ , leading to more frequent, intense, and  
57 longer-lasting acidification events (Hales et al., 2016; Harris et al., 2013). In the face of rapidly  
58 changing coastal conditions, tracking and quantifying the progression of OA requires precise and  
59 accurate measurements of carbonate chemistry over long periods of time; these can be achieved  
60 by appropriately constraining the carbonate system by measuring at least two of the system's  
61 parameters: total dissolved inorganic carbon ( $\text{TCO}_2$ ), total alkalinity (TA), pH, and the partial  
62 pressure of  $\text{CO}_2$  ( $p\text{CO}_2$ ). Despite the marked increase in OA research over the past decade  
63 (Riebesell and Gattuso, 2015; Rudd, 2017), nearshore monitoring efforts—particularly in  
64 estuarine waters—have been slow to ramp up, however, efforts are beginning to intensify as  
65 technological advancements are made (Feely et al., 2010, 2016; Hales et al., 2016; Harris et al.,  
66 2013; Newton et al., 2012; Waldbusser and Salisbury, 2014; Chan et al., 2017).

67  
68 Acidification of Alaskan coastal waters is predicted to progress rapidly relative to other  
69 regions within the next 50 years, and negatively impact the social-ecological structure of Alaskan  
70 marine resources by disrupting the Alaska Native subsistence and commercial fisheries (Ekstrom  
71 et al., 2015; Mathis et al., 2015b). The ocean waters present along the Alaskan coastline  
72 experience chemical and physical drivers of seawater chemistry that are unique to this region.  
73 The low seawater temperatures inherently have higher concentrations of dissolved  $\text{CO}_2$ , and  
74 chemical and physical oceanic processes unique to Alaskan waters such as sea ice melt, glacial  
75 discharge, and benthic pelagic coupling across shallow shelves are likely to exacerbate  
76 acidification in this region (Evans et al., 2014; Mathis et al., 2011a, 2011b, 2012). Recently, an  
77 OA monitoring initiative has been setup by the Alaska Ocean Observing Network (AOOS) to  
78 track and provide accessible material dedicated to acidification research in Alaskan waters  
79 (<http://www.aos.org/alaska-ocean-acidification-network>). Along the Pacific coast of Alaska, a  
80 robust benchtop system known as a Burke-o-Lator (BoL), which measures  $\text{TCO}_2$  and  $p\text{CO}_2$   
81 either continuously in a flow-through environment or from discrete seawater samples (Bandstra  
82 et al., 2006; Barton et al., 2012; Hales et al., 2016) has been installed in several locations,  
83 including the OceansAlaska Shellfish Hatchery in Ketchikan, the Alutiiq Pride Shellfish  
84 Hatchery in Seward (Evans et al., 2015), and at the Sitka Tribe of Alaska Environmental  
85 Research Center (real-time data from Alaskan and other BoLs:  
86 [http://www.ipacoa.org/Explorer?action=oiw:fixed\\_platform](http://www.ipacoa.org/Explorer?action=oiw:fixed_platform)). Nominal analytical uncertainty for  
87  $\text{TCO}_2$  determinations from this system is 0.2% based on the reproducibility of sample and  
88 certified reference material (CRM; provided by A. Dickson analyses). For  $p\text{CO}_2$  determinations,  
89 analytical uncertainty is 1.5% based on the inaccuracy of calculated CRM alkalinity relative to  
90 the certified value. While the BoL has significant advantages for achieving robust OA  
91 measurements in nearshore waters, the physical constraints of a benchtop system limit the spatial  
92 dimension of which carbonate chemistry parameters can be measured. One potential resolution

93 to diminish the gap in coverage of OA monitoring is to utilize autonomous pH sensors, which are  
94 far more versatile in their ability to monitor hard-to-reach areas.

95  
96 Recent assessments regarding OA monitoring efforts have specifically highlighted the  
97 benefits of accessibility by the commercially produced SeaFET<sup>TM</sup> pH sensor utilizing Honeywell  
98 Durafet technology (Martz et al., 2015). The SeaFET<sup>TM</sup> was originally developed at the  
99 Monterey Bay Aquarium Research Institute (Martz et al., 2010), but since has been  
100 manufactured and distributed by Satlantic (<http://www.satlantic.com>), which is now incorporated  
101 into Sea-Bird Scientific (<http://www.seabird.com>). The partnership between MBARI, Scripps  
102 Institute of Oceanography, and Satlantic led the way for commercial availability of the  
103 SeaFET<sup>TM</sup>, providing a ready-to-deploy-factory calibration, quick start manual, and user-friendly  
104 interface. The first generation of SeaFETs<sup>TM</sup> (not distributed by Sea-Bird, but by Dr. Todd Martz  
105 at Scripps Institute of Oceanography) have been deployed in numerous field studies and were  
106 heavily scrutinized in order to provide robust best practices for appropriate calibration and  
107 deployment procedures (Bresnahan et al., 2014; Hofmann et al., 2011; Kapsenberg and  
108 Hofmann, 2016; Martz et al., 2010; Matson et al., 2011; Yu et al., 2011). More recent studies  
109 have expanded the scope of SeaFET<sup>TM</sup> accuracy, inter-sensor variability, operator experience,  
110 and multi-point calibration techniques (Gonski et al., 2018; Johnson et al., 2017; Kapsenberg et  
111 al., 2017; McLaughlin et al., 2017). Given the multitude of information regarding SeaFET<sup>TM</sup>  
112 performance, coalescing all the potential sources of uncertainty in measurements (e.g., inter-  
113 sensor variability and calibration method) can be logistically challenging for non-experienced  
114 oceanographers who now have access to the commercially available SeaFETs<sup>TM</sup> distributed by  
115 Sea-Bird.

116  
117 In this study, we aimed to take advantage of two distinct coastal settings in order to  
118 deploy and evaluate the commercially available Sea-Bird SeaFET<sup>TM</sup>, and the potential  
119 uncertainties that can arise with time series pH<sub>t</sub> (total scale) measurements. For this evaluation,  
120 SeaFETs<sup>TM</sup> were co-deployed side-by-side to quantify inter-sensor variability, discrepancies  
121 were examined between factory calibration, *in situ* single-point calibration, and *in situ* multi-  
122 point calibration pH<sub>t</sub> values, and anomalous data associated with SeaFET<sup>TM</sup> conditioning times  
123 were detailed and considered as potential sources of measurement inaccuracies. All evaluations  
124 of SeaFET<sup>TM</sup> performance were under non-controlled source water conditions (i.e., non-  
125 manipulated seawater) or by *in situ* deployments. Three SeaFETs<sup>TM</sup> were deployed in coastal  
126 waters and were subjected to tidal influences and freshwater input, while a fourth was compared  
127 to pH<sub>t</sub> values derived from measurements obtained by a BoL. Finally, a spectral analysis of the  
128 quality-controlled data was performed in order to identify the driving mechanism of pH<sub>t</sub>  
129 variability between these divergent sites and consider possible un-accounted for calibration  
130 errors that could occur in dynamic settings that might not be resolved using a specific calibration  
131 method.

## 132 133 **2 Methods**

### 134 135 **2.1 Apparatus: SeaFET<sup>TM</sup>**

136  
137 The commercially available Sea-Bird SeaFET<sup>TM</sup> has retained the basic design of the original  
138 SeaFET<sup>TM</sup> developed at MBARI (Martz et al., 2010). The SeaFET<sup>TM</sup> utilizes the ion sensitive

139 field effect transistor (ISFET) technology, and is outfitted with an internal Honeywell Durafet  
 140 and an external solid-state chloride selective electrode (Cl-ISE) along with an internal thermistor,  
 141 which derives temperature using the (Steinhart and Hart, 1968) equation. The internal reference  
 142 electrode is intrinsically insensitive to salinity over a tested range from 30 – 36 (Bresnahan et al.,  
 143 2014), with recent work even suggesting near-ideal Nernstian response to salinity as low as ~9.0  
 144 (Gonski et al., 2018). This is in converse to the chloride sensitive external electrode, which is  
 145 salinity dependent. Both electrodes demonstrate exceptional stability over a range of moderate  
 146 salinity (30 – 36) and broad temperature (-1 to 35 °C) (Bresnahan et al., 2014; Kapsenberg et al.,  
 147 2015; Martz et al., 2014, 2010). The range of salinity sensitivity for the external electrode has  
 148 even been extended down to 20, where it displays a near-ideal Nernst slope (Takeshita et al.,  
 149 2014). Sea-Bird suggests that the external reference electrode provides the more accurate and  
 150 stable  $pH_t$  measurement given that chloride concentration can be precisely determined from  
 151 accurate salinity measurements. This is in agreement with previous research demonstrating that  
 152 the external electrode has a more robust stability (Martz et al., 2010). In dynamic nearshore  
 153 environments (e.g., estuaries with strong tidal and riverine fluxes), however, the  $pH_t$  derived  
 154 from the internal electrode is recommended (Sea-Bird Scientific’s Branham, C., pers. comm.)  
 155 despite the potential of thermodynamic hysteresis (Martz et al., 2010). Bresnahan et al. (2014)  
 156 demonstrated that the internal electrode is of the highest quality and under most scenarios  
 157 remains nearly as stable as the external electrode—this was further corroborated by Gonski et al.  
 158 (2018) with SeapHOx deployments in the Murderkill estuary, Delaware.

## 159 160 2.2 Calibration

161  
 162 Currently, three different calibration methods are present for the SeaFET<sup>TM</sup>: a factory pre-  
 163 deployment single-point calibration, *in situ* single-point calibration, and an *in situ* multi-point  
 164 calibration (Bresnahan et al., 2014; Gonski et al., 2018). To properly calculate  $pH_t$  from  
 165 SeaFET<sup>TM</sup> voltage readings, an appropriate calibration coefficient is required. The applied  
 166 calibration coefficients from the factory are a single-point, pre-deployment calibration. Given  
 167 that a conditioning period is required for the SeaFET<sup>TM</sup> (Bresnahan et al., 2014), these  
 168 coefficients are likely not adequate once the sensor becomes conditioned to the environment to  
 169 which it is deployed. For the internal electrode, the new calibration coefficient  $k_{0i}$  can be  
 170 determined as

$$171 \quad k_{0i} = -S_{Nernst} * pH_t + V_{int} - k_{2i} * T, \quad (1)$$

172  
 173 and  $k_{0e}$  for the external electrode

$$174 \quad k_{0e} = V_{ext} - pH_t + \log\left(1 + \frac{S_t}{K_s}\right) - 2 * \log(\gamma_{HCl}) - \log(Cl_T) * S_{nernst} + k_{2e} * T \quad (2)$$

175  
 176  
 177 where  $V_{FET}$  is the voltage from the electrode and  $k_2$  is the temperature coefficient ( $dE^*/dT$ )  
 178 applied to all SeaFETs<sup>TM</sup> (Martz et al., 2010). For detailed definitions of  $S_{nernst}$  and the salinity  
 179 dependent constants  $\gamma_{HCl}$  (HCl activity coefficient),  $Cl_T$  (total chloride),  $S_T$  (total sulfate), and the  
 180  $HSO_4^-$  dissociation constant  $K_s$  (Dickson et al., 2007; Khoo et al., 1977) in equations 1 and 2, we  
 181 refer readers to Martz et al. (2010), Bresnahan et al. (2014), and Sea-Bird Scientific SeaFET<sup>TM</sup>  
 182 Product Manual 2.0.0. In the literature, SeaFET<sup>TM</sup> calibration coefficients have been denoted as  
 183  $E_{int}^*$  and  $E_{ext}^*$  (Martz et al. 2010, Bresnahan et al. 2014), however, for the purpose of this

185 evaluation—which specifically examines commercially available Sea-Bird SeaFETs™—the  
186 adoption of  $k_0$  and  $k_2$  is in accordance with the preferred nomenclature from the manufacturer.

187  
188 Unlike the factory pre-deployment single-point calibration, the *in situ* single-point  
189 calibration occurs after the sensor has been deployed in the field. At the operator’s discretion, a  
190 discrete sample will be collected in direct proximity to the deployed SeaFET™ at the same time  
191 that the sensor is actively making a measurement, and then measured for  $\text{pH}_t$  at *in situ*  
192 temperature and salinity. The known  $\text{pH}_t$  would then be used in the above equations as the “ $\text{pH}_t$ ”  
193 variable. Similar to the single-point *in situ* calibration, the multi-point calibration derives a series  
194 of calibration coefficients over a short period of time that is long enough to capture environment  
195 variability such as tidal fluxes, and then a single calibration coefficient is averaged. Both single-  
196 point calibration methods—pre-deployment and *in situ*—appear to be suitable for fairly static  
197 environmental conditions, whereas the multi-point *in situ* calibration is best suited for dynamic  
198 nearshore environments (Bresnahan et al., 2014; Gonski et al., 2018).

### 200 2.3 SeaFET™ conditioning: test tank deployments

201  
202 A series of three separate test tank deployments for three SeaFETs™<sub>395, 396, 397</sub> were conducted in  
203 order to determine the conditioning period for each sensor. Initial sensor deployments took place  
204 in October 2016 at the Alutiiq Pride Shellfish Hatchery (APSH) in Seward, Alaska. Sensors were  
205 deployed for a duration of 72 hours in a flow-through 60 L tank where seawater taken from a  
206 depth of ~75 m in Resurrection Bay was sand-filtered, UV treated, and finally run through a 5  
207  $\mu\text{m}$  mesh. All three sensors were programmed with identical sampling settings (Table 1). The  
208 onboard internal thermistor was used to calculate temperature, and measurements of seawater  
209 salinity incoming to the hatchery were collected by a Sea-Bird Scientific SBE 45 MicroTSG  
210 Thermosalinograph that is paired with the BoL and are available on the Alaska Ocean Observing  
211 System (<http://portal.aooos.org/real-time-sensors.php#map>). Factory calibration coefficients for  
212 the internal ( $k_{0i}$ ,  $k_{2i}$ ) and external ( $k_{0e}$ ,  $k_{2e}$ ) electrodes were retained when processing raw voltage  
213 data.

214  
215 A second tank deployment for the same three SeaFETs™<sub>395, 396, 397</sub> were deployed at the  
216 University of Alaska, Fairbanks, in the Ocean Acidification Research Center (OARC). Seawater  
217 collected from the APSH was delivered to the OARC test tank, ~370 L in a half-filled tank.  
218 Seawater in the tank was circulated continuously and covered to aid in the prevention of  
219 evaporation and photosynthesis. A co-deployed Sea-Bird SBE 16plusV2 SeaCAT (recently  
220 serviced by Sea-Bird) collected temperature and salinity readings every 5 minutes.  
221 SeaFETs™<sub>395, 396, 397</sub> were deployed for a duration of nine days in continuous operation mode  
222 which forgoes the ability to set frames per burst; average number of reads was identical between  
223 all sensors (Table 1). From 1 – 4 November 2016, duplicate discrete bottle samples were  
224 collected in 250 ml glass bottles with screw caps at ~00:00 and 17:00 UTC per day. Bottle  
225 samples were preserved with 20  $\mu\text{l}$  of saturated  $\text{HgCl}_2$  and processed at a later date for  $\text{TCO}_2$  and  
226 TA with a VINDTA 3C (Versatile Instrument for the Determination of total inorganic carbon  
227 and titration alkalinity). The VINDTA 3C has an uncertainty typically near 0.05% (Mathis et al.,  
228 2014, 2015a). Bottle sample  $\text{pH}_t$  was calculated using CO2SYS with known  $\text{TCO}_2$  and TA using  
229 the constants provided by (Uppström, 1974) and (Lueker et al., 2000); derived  $\text{pH}_t$  was then  
230 compared against SeaFET™ sensor  $\text{pH}_t$  to test the accuracy of both internal and external

231 electrodes, assuming the discrete bottle samples were the “true pH” of the seawater. Upon  
232 recovery, all SeaFETs<sup>TM</sup><sub>395, 396, 397</sub> were placed into polled mode and stored with wet caps filled  
233 with tris buffer (salinity 34, pH 8.09 at room temperature, 25 °C). Again, the factory calibration  
234 coefficients for the internal and external electrodes were retained when raw voltage was  
235 processed. Since the SBE 16plusV2 sampled every 5 min, salinity and temperature measured by  
236 the SBE at each 5-minute point was repeated for the following 4 minutes in order to calculate  
237 continuous minute readings by SeaFETs<sup>TM</sup><sub>395, 396, 397</sub>.

238  
239 A final test tank deployment of the SeaFETs<sup>TM</sup><sub>395, 396, 397</sub> at OARC was conducted after an  
240 assumed adequate conditioning period of nine days (first OARC deployment). All three  
241 SeaFETs<sup>TM</sup><sub>395, 396, 397</sub> had been set to polled mode after the end of the previous deployment and,  
242 therefore, were sleeping for 83 days until this final seven day deployment. The sampling settings  
243 were identical to the first OARC deployment for all three SeaFETs<sup>TM</sup><sub>395, 396, 397</sub> (Table 1). Similar  
244 to the previous OARC tank deployment, a co-deployed Sea-Bird SBE 16plusV2 SeaCAT  
245 collected temperature and salinity mirroring the SeaFET sampling interval of 3 hrs.

246  
247 The internal thermistor of each SeaFET<sup>TM</sup><sub>395, 396, 397</sub> was tested for accuracy by comparing  
248 its derived *in situ* temperature to that collected by the Sea-Bird SBE 16plusV2 during the test  
249 tank deployments. The temperature difference between the internal thermistor and the SBE  
250 16plusV2 was used to calculate the average and maximum discrepancy between the two  
251 temperature readings. The temperature discrepancy was then applied to a combination of TA:  
252 TCO<sub>2</sub> ratios over a range of salinity (20 – 35) in CO2SYS (constants: Uppström, 1974; Lueker et  
253 al., 2000), which produced two different pH<sub>t</sub> values. The difference between these two pH<sub>t</sub>  
254 values were, therefore, concluded to be a result of the temperature discrepancy.

## 255 256 **2.4 SeaFET<sup>TM</sup> performance: field deployments**

257  
258 In late boreal winter 2017—32 days post final tank deployment—SeaFET<sup>TM</sup><sub>397</sub> was deployed at  
259 the APSH and the two remaining sensors (SeaFET<sup>TM</sup><sub>395, 396</sub>) in Kasitsna Bay within greater  
260 Kachemak Bay, Alaska (Fig. 1). At the APSH (60° 5' 55.59"N, 149° 26' 39.80"W), incoming  
261 seawater from Resurrection Bay at a depth of 75 m is split before running through a series of  
262 hatchery water filters so that an unfiltered line is run directly to the BoL. The incoming line to  
263 the BoL was then split to feed an ~11.5 L conical tank housing the SeaFET<sup>TM</sup><sub>397</sub> fit with the  
264 copper bio-fouling guard; tank residence time was ~7.5 min. The SeaFET<sup>TM</sup><sub>397</sub> at this location  
265 was deployed on 6 March 2017 with a robust sampling setting (Table 1). Two calibration  
266 methods were applied for this SeaFET<sup>TM</sup><sub>397</sub>, an *in situ* single-point calibration and an *in situ*  
267 multi-point calibration. Both calibrations were performed 50 days after deployment on 25 April  
268 2017 once the BoL had completed service maintenance. The single-point *in situ* calibration was  
269 taken during midday tide transition in Resurrection Bay, while the multi-point *in situ* approach  
270 used five (sensor sampling 3 h intervals) time points spanning an entire tidal cycle. The single-  
271 point *in situ* calibration was used to derive  $k_{0i}$  for the internal electrode (eq. 1) and  $k_{0e}$  for the  
272 external electrode (eq. 2). The multi-point *in situ* calibration followed the same formulations  
273 with the difference being the final calibration coefficient calculated was the average of the five  
274 independently calculated calibration coefficients. Three final pH<sub>t</sub> values for the SeaFET<sup>TM</sup><sub>397</sub>  
275 were, therefore, calculated based upon the different calibration coefficients (factory, single-point  
276 and multi-point *in situ* calibration) and compared against the pH<sub>t</sub> determined from continuous

277  $p\text{CO}_2$  measurements by the BoL and derived TA (TA-S equation, Evans et al. 2015) using  
278 CO2SYS with constants provided by Uppström (1974) and Lueker et al. (2000).  $\text{pH}_t$  uncertainty  
279 from the BoL using this combination of measured and derived parameters is 0.007 units based on  
280 propagating the error of the BoL  $p\text{CO}_2$  uncertainty reported above with the RMSE ( $17 \mu\text{mol kg}^{-1}$ )  
281 of the regional TA-S relationship (Orr, et al., *in prep*).

282  
283 Inter-sensor variability was examined between two SeaFETs<sup>TM</sup><sub>395,396</sub> deployed off the  
284 pier at the Kasitsna Bay laboratory in Kachemak Bay ( $59^\circ 28' 6.71''\text{N}$ ,  $151^\circ 33' 11.12''\text{W}$ )  $\sim 1.5$  m  
285 from the bottom: depth at this location fluctuates between  $\sim 7.5 - 16.8$  m (Fig. 1). On 18 March  
286 2017—44 days post final tank deployment—SeaFETs<sup>TM</sup><sub>395,396</sub> were attached to the pier piling  
287 directly beside one another on a single mooring frame. Both SeaFETs<sup>TM</sup> were wrapped with pipe  
288 tape to minimize biofouling and fit with their respective copper biofouling guards which had a  
289 tributyltin plug attached to the inside of the guard. The sampling settings for both SeaFETs<sup>TM</sup><sub>395,</sub>  
290 <sub>396</sub> were identical to the one at the APSH (Table 1). Five discrete reference samples were taken in  
291 duplicate: one sample on day of deployment (UTC: 3-18-17, 18:00), two samples 1-day post-  
292 deployment (UTC: 19 March 2017, 03:00 and 15:00), and two samples 2- and 1-day pre-  
293 recovery of the SeaFETs<sup>TM</sup><sub>395,396</sub> (UTC 3 June 2017, 03:00; 6 June 2017, 03:00). Reference  
294 samples were collected within 30 s of the instrument sampling time period via a diver's hand  
295 Niskin, measured for temperature and salinity with a YSI 3100 conductivity instrument, stored in  
296 250 ml glass bottles with screw caps, poisoned with 100  $\mu\text{l}$  of saturated  $\text{HgCl}_2$ , and secured with  
297 teflon tape around the bottleneck threading and Parafilm wrapped on the outside of the cap.  
298 Calibration samples were processed for  $\text{TCO}_2$  and TA with a VINDTA 3C and  $\text{pH}_t$  calculated  
299 using CO2SYS with the constants provided by Uppström (1974) and Lueker et al. (2000).  
300 Salinity measurements collected by the Kachemak Bay National Estuarine Research Reserve  
301 data sonde, 10 km SE of the deployed sensors ( $59^\circ 26' 26.87''\text{N}$ ,  $151^\circ 43' 15.21''\text{W}$ ), were used  
302 along with the SeaFET's<sup>TM</sup> internal thermistor readings to calculate  $\text{pH}_t$  from the raw voltage  
303 data in order to capture representative environmental conditions providing relevance for the  $\text{pH}_t$   
304 time series in this location. A static salinity of 32 was also used for all calculations of  $\text{pH}_t$  as an  
305 assessment of variability due to salinity measured from a data sonde 10 km away. A total of four  
306 different  $\text{pH}_t$  values for both SeaFETs<sup>TM</sup><sub>395,396</sub> were calculated based on calibration method  
307 (factory pre-deployment single-point calibration and the *in situ* single-point) and conditioning:  
308 either conditioned or non-conditioned to the environment. All calculated  $\text{pH}_t$  values from the  
309 SeaFETs<sup>TM</sup><sub>395,396</sub> were then compared against the remaining discrete reference bottle samples  
310 not used for calibration. This was done in order to examine the accuracy and inter-sensor  
311 variability difference between conditioned and non-conditioned to the environment electrodes.  
312 Because the Kachemak Bay data sonde was located 10 km from the deployed SeaFETs<sup>TM</sup><sub>395,396</sub>,  
313 the measured temperature and salinity from the discrete reference samples were used to  
314 determine  $\text{pH}_t$  for the internal and external electrodes at those specific time points. That is,  
315 sensor accuracy for these two SeaFETs<sup>TM</sup><sub>395,396</sub> was only assessed with accurate temperature and  
316 salinity values determined from the discrete bottle samples.

317  
318 A fourth SeaFET<sup>TM</sup><sub>268</sub> operated by the Hakai Institute was deployed on Environment  
319 Canada's Sentry Shoal weather buoy in the Northern Strait of Georgia, BC, Canada:  $49^\circ 54'$   
320  $24.00''\text{N}$ ,  $124^\circ 59' 5.99''\text{W}$  (Fig.1). The Sentry Shoal mooring site is in a water depth of 15 m and  
321 the SeaFET<sup>TM</sup><sub>268</sub> was affixed at a depth of 1 m. A pre-deployment bucket test was conducted for  
322 24 h at a sampling interval of 30 min with an average of 10 samples per frame and 30 frames per

323 burst from 28 – 29 June 2016. SeaFET<sup>TM</sup><sub>268</sub> was outfitted with a copper housing guard and  
 324 wrapped with copper tape. Sensor underwent two separate deployments, an initial deployment,  
 325 and a redeployment (6 July and 27 August 2016) that occurred after the sensor was retrieved for  
 326 cleaning and maintenance. Two separate calibration samples (taken in triplicate) were taken in  
 327 accordance with each deployment, and occurred 13 and 7 days after each deployment (19 July  
 328 and 2 September 2016). For each deployment, SeaFET<sup>TM</sup><sub>268</sub> settings were similar to the others at  
 329 the APSH and in Kasitsna Bay (Table 1). All calibration samples were taken in triplicate at a  
 330 depth of 1 m via CTD and Niskin bottle castings and collected in 350 ml amber glass bottles with  
 331 polyurethane-lined crimp-sealed metal caps and poisoned with 200 µl of saturated HgCl<sub>2</sub>, and  
 332 then processed for TCO<sub>2</sub> and pCO<sub>2</sub> with a BoL at the Hakai Institute’s Quadra Island Field  
 333 Station. The measured values were used to derive pH<sub>t</sub> using CO2SYS with the constants  
 334 provided by (Uppström, 1974) and (Lueker et al., 2000) in order to perform a single-point *in situ*  
 335 calibration. Uncertainty in pH determinations from BoL pCO<sub>2</sub> and TCO<sub>2</sub> measurements was  
 336 0.006 units. After SeaFET<sup>TM</sup><sub>268</sub> deployment and calibration, a total of three, triplicate, reference  
 337 sample sets were taken and processed for pH<sub>t</sub> following the procedure used for calibration  
 338 samples, then compared against SeaFET pH<sub>t</sub>.

## 339 2.5 Quantifying pH<sub>t</sub> and intrinsic sensor uncertainties

340  
 341 Calculating pH<sub>t</sub> from the SeaFET’s<sup>TM</sup> raw voltage reading is dependent on temperature, salinity  
 342 and an ideal 100% Nernstian response. The software application SeaFETcom permits the  
 343 operator to automatically calculate pH<sub>t</sub> by assigning the calibration coefficient either written to  
 344 the sensor’s header file or the one provided on the CD-ROM (these should be identical).  
 345 Determination of final pH<sub>t</sub> values from the first test tank deployment at the APSH were  
 346 calculated by two different operators and two sources for the factory pre-deployment single-point  
 347 calibration coefficients: header file and CD-ROM disc file. Aside from that exception, all other  
 348 final pH<sub>t</sub> values for the internal and external electrodes were calculated with the Mathworks  
 349 software MATLAB (V. 2016a) and Microsoft excel (v. 2016) using the following equations for  
 350 the internal electrode

$$352 \quad pH_{int} = \frac{V_{FET|INT} - k_{0i} - k_{2i} * T}{S_{nernst}}, \quad (3)$$

353 and the external electrode

$$354 \quad pH_{ext} = \frac{V_{FET|EXT} - k_{0e} - k_{2e} * T}{S_{nernst}} + \log(Cl_T) + 2 * \log(\gamma_{HCl}) - \log\left(1 + \frac{S_t}{K_s}\right) \quad (4)$$

355 where V<sub>FET</sub> is the voltage from the electrode and k<sub>2</sub> is the temperature coefficient (dE\*/dT)  
 356 applied to all SeaFETs<sup>TM</sup> (Martz et al. 2010). Again, for detailed definitions of S<sub>nernst</sub> and the  
 357 salinity dependent constants γ<sub>HCl</sub> (HCl activity coefficient), Cl<sub>T</sub> (total chloride), S<sub>T</sub> (total sulfate),  
 358 and the HSO<sub>4</sub><sup>-</sup> dissociation constant K<sub>s</sub> (Khoo et al. 1977, Dickson et al. 2007) in equations 3 and  
 359 4, we refer readers to Martz et al. (2010), Bresnahan et al. (2014), and Sea-Bird Scientific  
 360 SeaFET<sup>TM</sup> Product Manual 2.0.0.

### 361 2.5.1 Sensor uncertainty

362 The overall accuracy of every SeaFET<sup>TM</sup> sensor was evaluated by quantifying all sources of



363 potential uncertainty when calculating a final  $\text{pH}_t$  from the SeaFET<sup>TM</sup> (Table 2). The  $\text{pH}_t$   
364 uncertainty introduced by calibration method was calculated as the absolute difference between  
365 the “true  $\text{pH}_t$ ” and the final sensor  $\text{pH}_t$  derived from either factory calibration, the single-point *in*  
366 *situ* calibration, or multi-point *in situ* calibration. The “true  $\text{pH}_t$ ” was calculated using CO2SYS  
367 dissociation constants by Lueker et al., (2000) and Uppström, (1974) with measured  $\text{TCO}_2$  and  
368 TA via the VINDTA 3C,  $\text{TCO}_2$  and  $\text{pCO}_2$  measured by the BoL for discrete samples (e.g.,  
369 SeaFET<sup>TM</sup><sub>268</sub>), and  $\text{pCO}_2$  and TA (TA-S equation, Evans et al. 2015) for continuous samples  
370 (SeaFET<sup>TM</sup><sub>397</sub>). A one-way analysis of variance (ANOVA) and the root mean square error  
371 (RMSE) were run and calculated in order to compare the  $\text{pH}_t$  values from both electrodes on  
372 SeaFET<sup>TM</sup><sub>397</sub> across calibration methods against the  $\text{pH}_t$  values from the BoL. The BoL at the  
373 APSH sampled every 5 min which produced 256 comparable sample points with a time  
374 alignment disparity that ranged from 0 – 120 s against SeaFET<sup>TM</sup><sub>397</sub>. The potential  $\text{pH}_t$   
375 uncertainty based on the thermistor was calculated by using the absolute difference between the  
376 thermistor derived temperature and that measured by the SBE 16plusV2 ( $T_{\text{diff}}$ ) from the OARC  
377 test tank deployments and the Kasitsna Bay SeaFETs<sup>TM</sup><sub>395, 396</sub> against the Seldovia data sonde 10  
378 km away. Finally, an average inter-sensor variability uncertainty term was calculated as the  
379 difference between the two SeaFETs<sup>TM</sup><sub>395, 396</sub> deployed side-by-side in Kasitsna Bay after a  
380 single-point *in situ* calibration was performed. All uncertainty terms were calculated and collated  
381 based on our evaluations from the Alaska deployed SeaFETs<sup>TM</sup><sub>395, 396, 397</sub>, while SeaFET<sup>TM</sup><sub>268</sub>  
382 deployed at Sentry Shoal was only included when determining the accuracy uncertainty term.  
383 Due to the disparity between reference samples for the Kasitsna Bay SeaFETs<sup>TM</sup><sub>395, 396</sub> and  
384 Sentry Shoal SeaFET<sup>TM</sup><sub>268</sub> (two discrete reference samples) to that at the ASPH SeaFET<sup>TM</sup><sub>397</sub>  
385 (256 reference samples), only the average calculated difference (SeaFET<sup>TM</sup>  $\text{pH}_t$  – “true  $\text{pH}_t$ ”) for  
386 each calibration method and electrode was used from the APSH SeaFET<sup>TM</sup><sub>397</sub> and then collated  
387 with the other reference points from the Kasitsna Bay and Sentry Shoal SeaFETs<sup>TM</sup><sub>395, 396, 268</sub>.

## 388 2.5.2 $\text{pH}_t$ time series analysis

389  
390 Final time series analysis was examined in the time and frequency domain using the Mathworks  
391 software MATLAB (V. 2016a). Power spectral density was determined via Welch’s method  
392 using the pwelch function in MATLAB. Time series data was resampled and linearly  
393 interpolated in order to compensate for the missing data points that occurred when sensors  
394 arbitrarily stopped sampling.

395

## 396 3 Results

397

### 398 3.1 Test tank and field conditions

399

400 Finalized (i.e., calibrated)  $\text{pH}_t$  values from the first test tank deployment produced two different  
401 values, of which each was dependent on whether the calibration coefficient from the header file  
402 or the disc file was selected, the result was a difference of ~0.0011 units for both the internal and  
403 external electrodes. Because sensors were stored in tris buffer that lacked the addition of bromide  
404 between tank deployments and before field deployments, an environmental conditioning period  
405 was required for each of the Alaska SeaFETs<sup>TM</sup><sub>395, 396, 397</sub> once submerged in their respective  
406 field sites. Thus, any determination of SeaFET<sup>TM</sup>  $\text{pH}_t$  accuracy and conditioning period from

407 tank deployments were inconclusive and will not be considered henceforth. No SeaFETs<sup>TM</sup><sub>395, 396,</sub>  
408 <sub>397, 268</sub> displayed signs of biofouling or low battery power upon recovery.

409  
410 SeaFET<sup>TM</sup><sub>397</sub> deployed in parallel with the BoL at the APSH experienced a tank failure  
411 on 8 April 2017 resulting in the sensor's emergence for 24 h. In addition, missing temperature  
412 and salinity values resulted in gaps of pH<sub>t</sub> measurements over the entire deployment. The BoL  
413 experienced flow control issues when initial deployment occurred on 6 March 2017 and was not  
414 online until 18 April 2017 but, then, operated nearly consistently until 24 May 2017. All pH<sub>t</sub> and  
415 temperature comparisons were, therefore, made beginning on 18 April 2017.

416  
417 Due to the *in situ* environmental conditioning period of the Kasitsna Bay SeaFETs<sup>TM</sup><sub>395,</sub>  
418 <sub>396,</sub> calibration was performed using the initial reference sample collected on 18 March 2017,  
419 03:00 UTC and again with the reference sample collected on 3 June 2017, 03:00 UTC. Due to  
420 high variance between duplicate reference samples (SD: 0.08 pH<sub>t</sub>) on 19 March 2017, 15:00  
421 UTC, this reference was discarded and not used for comparison or calibration. The Sentry Shoal  
422 SeaFET<sup>TM</sup><sub>268</sub> underwent one maintenance and cleaning procedure, including a battery change,  
423 during the ~5-month deployment (Table 1). One calibration sample (19 July 2016) and one  
424 reference sample (9 November 2016) were averaged from duplicate rather than triplicate  
425 replicates due to large variance from one of the replicate samples. The reference sample taken on  
426 23 August 2016, 17:00 UTC was discarded as temperature and salinity data were missing and  
427 SeaFET<sup>TM</sup><sub>268</sub> pH<sub>t</sub> could not be calculated. The final reference sample (UTC: 9 November 2016,  
428 17:05) was taken 5 min after SeaFET<sup>TM</sup><sub>268</sub> sampled on 9 November 2016, 17:00 UTC.

429

### 430 **3.2 Thermistor response: test tank deployment**

431

432 The internal thermistor amongst the SeaFETs<sup>TM</sup><sub>395, 396, 397</sub> had a difference of less than 0.2 °C  
433 over the entirety of the second and third tank deployments. All thermistor derived temperature  
434 values had good alignment with the SBE 16plusV2 temperature, and consistently recorded a  
435 slightly higher temperature. The discrepancy between the thermistor temperature and  
436 SBE16plusV2 was minimal, and reached a maximum of 0.378 (logged by SeaFET<sup>TM</sup><sub>395</sub>) during  
437 any time over all tank deployments. The average discrepancy, however, was ~0.21 °C when  
438 averaging across all SeaFETs<sup>TM</sup><sub>395, 396, 397</sub> and all times—resulting in a 0.003 pH uncertainty.

439

### 440 **3.3 Field performance**

441

442 SeaFET<sup>TM</sup><sub>397</sub> deployed alongside the BoL appeared stable throughout its entire deployment and  
443 tracked the pH<sub>t</sub> derived from the BoL well (Fig. 2). Errant spikes were present from both  
444 electrodes throughout periods before 18 April 2017, which were a result of plumbing changes  
445 that occurred to the APSH incoming seawater. On 10 April 2017 the internal thermistor, BoL  
446 temp, and BoL salinity fluctuated by 3 °C and 14, respectively, over a 12 h period. These  
447 anomalies were removed from analysis. Salinity remained relatively stable throughout the rest of  
448 the deployment and ranged from 30.0 – 32.1. The pH<sub>t</sub> uncertainty decreased, and the accuracy of  
449 the SeaFET's<sup>TM</sup><sub>397</sub> internal electrode improved once the *in situ* single-point and multi-point  
450 calibrations were performed with a RMSE decreasing from 0.5455 pH<sub>t</sub> units under factory  
451 calibration, 0.0361 pH<sub>t</sub> units for *in situ* single-point calibration and 0.0273 pH<sub>t</sub> units for the *in*  
452 *situ* multi-point calibration. The external electrode also improved accuracy with *in situ* single-

453 point and multi-point calibrations with an RMSE of 0.1077 under factory calibration, 0.0390 for  
454 *in situ* single-point calibration and 0.0388 for the *in situ* multi-point calibration (Fig. 2). There  
455 was a significant difference in the reduction of the  $\text{pH}_t$  uncertainty for both the internal and  
456 external electrodes when utilizing *in situ* single-point and multi-point calibration coefficients  
457 compared to the factory calibration coefficients (Table 3). In addition, there was a significant  
458 decrease in the  $\text{pH}_t$  uncertainty when using the *in situ* multi-point calibration coefficients rather  
459 than the *in situ* single-point method for the internal electrode, but not for the external electrode  
460 (Table 3). The  $\text{pH}_t$  uncertainty of the internal electrode decreased from 0.0294 units with an *in*  
461 *situ* single-point calibration to 0.0224 units after an *in situ* multi-point calibration. It should be  
462 noted that the time alignment disparity which ranged from 0 – 120 s is not considered a  
463 significant source of discrepancy as only 4 sample points out of the 256 comparable points were  
464  $> 0.03$  units (i.e., only 4 comparable points greater than the average  $\text{pH}_t$  uncertainty found after  
465 calibration) between any one 5 min sample taken by the BoL. The internal thermistor of  
466 SeaFET<sup>TM</sup><sub>397</sub> tracked the recorded BoL temperature trend fairly (Fig. 3), but had a greater  
467 magnitude discrepancy than its test tank deployment ( $\sim 0.21$  °C). On average, the thermistor  
468 temperature had an absolute difference of 2.83 °C (SD 0.35) from 18 April 2017 – 6 June 2017,  
469 which would result in a  $\text{pH}_t$  uncertainty of  $\sim 0.044$  units. SeaFET<sup>TM</sup><sub>397</sub> was not fully submerged in  
470 the conical tank leaving the top portion susceptible to air temperature fluctuations which could  
471 have affected the thermistor readings.

472

473 The SeaFETs<sup>TM</sup><sub>395, 396</sub> in Kasitsna Bay improved their accuracy after an *in situ* single-  
474 point calibration was performed (Fig. 4), however, this was only the case when sensors were not  
475 conditioned as calibration performed after the conditioning period reduced accuracy (Fig. 5)  
476 when comparing against discrete reference samples. It should be noted that only the  $\text{pH}_t$  recorded  
477 by both SeaFETs<sup>TM</sup><sub>395, 396</sub> at times of the reference samples had precise salinity and temperature  
478 (temperature and salinity recorded with reference sample rather than thermistor derived  
479 temperature) measurements as all other measurements were calculated from salinity measured by  
480 the data sonde 10 km away, and with temperature derived from the onboard thermistor. The  $\text{pH}_t$   
481 recorded by the external electrode at a fixed salinity displayed little to no variance relative to  $\text{pH}_t$   
482 calculated with data sonde salinity ( $< 0.02$   $\text{pH}_t$  difference: average whether conditioned or non-  
483 conditioned to environment). The average  $\text{pH}_t$  uncertainty from both SeaFETs<sup>TM</sup><sub>395, 396</sub> reduced  
484 by approximately half for the internal electrode when not conditioned to the environment after an  
485 *in situ* single-point calibration was performed (0.1072 and 0.1394 to 0.0475 and 0.0741 units,  
486 respectively), while the external electrode improved only minimally from 0.0988 and 0.0963 to  
487 0.0610 and 0.0894 units, respectively (Fig. 4). When *in situ* single-point calibration was  
488 performed after the SeaFETs<sup>TM</sup><sub>395, 396</sub> were conditioned (i.e., calibrated with reference sample  
489 taken on 4 June 2017, 03:00 UTC), the  $\text{pH}_t$  uncertainty for the internal electrode reduced only  
490 minimally from factory calibration: 0.1072 and 0.1394 to 0.0896 and 0.1240 units, respectively  
491 (Fig. 5a, b). Conversely, the  $\text{pH}_t$  error for the external electrode increased from 0.0988 and  
492 0.0963 to 0.1011 and 0.1480, respectively (Fig 5c, d).

493

494 Both SeaFETs<sup>TM</sup><sub>395, 396</sub> displayed low inter-sensor variability for the internal electrode,  
495 and high for the external electrode after *in situ* single-point calibration was performed on sensors  
496 not conditioned to the environment (Fig. 6, gray circles). The mean anomaly between both  
497 SeaFET's<sup>TM</sup><sub>395, 396</sub> internal electrodes was 0.0525 units, whereas the external mean anomaly was  
498 0.145 units. When measurements taken before the sensor was conditioned to the environment

499 (blue shaded region Fig. 6) were removed from analysis, the mean anomaly changed by  $< 0.006$   
500 units for both electrodes. Inter-sensor variability for both electrodes once conditioned, and after  
501 *in situ* single-point calibration, was  $< 0.05$  units: 0.0409 and 0.0461 units for the internal and  
502 external electrodes, respectively (Fig. 6, black circles). When measurements recorded before the  
503 sensors were conditioned to the environment were removed (blue shaded region Fig. 10), the  
504 anomaly decreased further,  $< 0.015$  units for both electrodes.  
505

506 Thermistor readings on both SeaFETs<sup>TM</sup><sub>395, 396</sub> tracked the temperature at the Seldovia  
507 site well, however errant spikes occurred around 18 April 2017 and again around 10 May 2017,  
508 and continued till the end of the deployment (Fig. 7). The absolute average difference between  
509 the thermistor values and the Seldovia data sonde was 0.281 °C (SD 0.295), nearly identical to  
510 the difference displayed during the test tank deployments, average 0.21 °C.  
511

512 At Sentry Shoal, temperature and salinity seasonally fluctuated and ranged from 8.71 –  
513 21.8 °C and 23.4 – 29.4, respectively. Based on the overall accuracy of the internal and external  
514 electrodes, there was no clear distinction as to which provided the more robust measurement  
515 after *in situ* single-point calibration was performed. While the external electrode did display a  
516 lower pH<sub>t</sub> average uncertainty, this was based on only two reference points, one of which had a  
517 time discrepancy of 5 min (9 November 2016, 17:05 UTC). Only two reference samples were  
518 comparable against SeaFET<sup>TM</sup><sub>268</sub> pH<sub>t</sub> due to the loss of salinity and temperature data on 23  
519 August 2016, 17:00 UTC. Reference samples on 26 September 2016 and 9 November 2016  
520 were, therefore, compared using the new calibration coefficients determined after redeployment  
521 on 27 August 2016. The average pH<sub>t</sub> uncertainty was  $< 0.0115$  units for both electrodes (Fig. 8)  
522 compared to average pH<sub>t</sub> uncertainties of 0.0244 and 0.0560 units for the internal and external  
523 electrodes, respectively, if initial calibration coefficients from 19 July 2016 were retained. The  
524 low pH<sub>t</sub> uncertainty ( $< 0.0137$  units) determined after the *in situ* single-point calibration,  
525 however, was still greater than the average pH<sub>t</sub> uncertainty under factory calibration:  $< 0.005$   
526 units for both electrodes (Fig 8).  
527

### 528 3.4 Spectral analysis

529  
530 All SeaFETs<sup>TM</sup><sub>395, 396, 397, 268</sub> displayed a mixed semi-diurnal tidal response during all field  
531 deployments (Fig. 9). SeaFETs<sup>TM</sup><sub>395, 396</sub> at Kasitsna Bay had a stronger amplitude response at a  
532 frequency of two cycles d<sup>-1</sup>, whereas SeaFET<sup>TM</sup><sub>397</sub> had a greater amplitude at one cycle d<sup>-1</sup> (Fig.  
533 9a, c, d). All three SeaFETs<sup>TM</sup><sub>395, 396, 397</sub> in Alaskan waters had a strong amplitude signal of 1  
534 cycle every 21 days, with an addition signal of one cycle every three days for SeaFET<sup>TM</sup><sub>397</sub>. The  
535 amplitude signal for SeaFET<sup>TM</sup><sub>397</sub> shifted depending on source of measurement (BoL, internal or  
536 external electrode), however, all measurement sources followed the same frequency pattern (Fig  
537 9a). SeaFET<sup>TM</sup><sub>268</sub> displayed a strong signal at a frequency of zero as well as at one and two  
538 cycles d<sup>-1</sup> (Fig 9a).  
539

### 540 3.5 Intrinsic uncertainty and accuracy

541  
542 Among the calculated potential sources of uncertainty in pH<sub>t</sub>, inter-sensor variability (difference  
543 between SeaFETs<sup>TM</sup> pH<sub>t</sub>) and sensor accuracy produced the greatest uncertainty discrepancies  
544 for the internal and external electrodes under factory calibration (Fig. 10). The pH<sub>t</sub> uncertainty

545 (i.e., overall sensor accuracy) for the internal electrode reduced a greater degree than the external  
546 electrode at every ordinal calibration method: factory, *in situ* single-point, to *in situ* multi-point  
547 calibration (Fig. 10). This was not the case for the external electrode, however, as the overall  $\text{pH}_t$   
548 accuracy was greater when factory calibration was used compared to an *in situ* single-point  
549 calibration was performed after the sensor was conditioned. The thermistor uncertainty (i.e.,  
550 uncertainty when calculating  $\text{pH}_t$  based on the thermistor temperature rather than a more accurate  
551 temperature gauge) produced a  $\text{pH}_t$  uncertainty of 0.0044 units, and was based on the recorded  
552 values by SeaFETs<sup>TM</sup><sub>395, 396</sub>. Even though the temperature-derived values from the thermistor of  
553 SeaFETs<sup>TM</sup><sub>395, 396</sub> were compared against a data sonde 10 km away, the average  $T_{\text{diff}}$  values were  
554 consistent with the  $T_{\text{diff}}$  calculated from the test tank deployments (within 0.07°C) and, therefore,  
555 provided an adequate resolution to determine a thermistor uncertainty value.

556

#### 557 4 Discussion

558

559 Obtaining accurate and precise measurements of pH in nearshore coastal waters is crucial for  
560 understanding changing trends, dynamics, and current baselines of acidification in these—  
561 “susceptible to change”—marine domains. For dynamic nearshore systems, the current standard  
562 of OA weather (carbonate chemistry variability on timescales of days to months) accuracy  
563 should have an uncertainty no greater than 0.02 pH units according to the Global Ocean  
564 Acidification Observing Network (Newton et al. 2015). Previous evaluations of the SeaFET<sup>TM</sup>  
565 sensor package have demonstrated accuracy for both electrodes to be better than 0.02 pH units,  
566 with a range between 0.01 – 0.04 units for the internal electrode in more dynamic environments  
567 (Bresnahan et al., 2014; Gonski, 2018; Martz et al., 2010). Based on our findings, we observed  
568 an accuracy range of 0.009 – 0.148  $\text{pH}_t$  units after sensors were conditioned and *in situ* single-  
569 point or multi-point calibrations were performed for the internal and external electrodes. This  
570 range decreased when SeaFETs<sup>TM</sup><sub>395, 396</sub> from Kasitsna Bay were calibrated with reference  
571 samples taken at initial deployment (i.e., non-conditioned to environment). For SeaFET<sup>TM</sup><sub>397</sub>, the  
572 internal electrode’s accuracy was nearly identical to that of the external electrode after an *in situ*  
573 multi-point calibration (Fig. 2), suggesting that the internal electrode can produce a highly  
574 precise  $\text{pH}_t$  measurement comparable to the BoL with an accuracy meeting the standards of the  
575 OA weather measurements (Newton et al. 2015). This is not to suggest that the SeaFET<sup>TM</sup> can  
576 replace the BoL, particularly because the BoL can capture multiple carbonate chemistry  
577 measurements thereby fully constraining the system and identifying potential decoupling of the  
578 carbonate system in estuarine waters (Bandstra et al., 2006; Hales et al., 2016). Nonetheless, the  
579 SeaFET<sup>TM</sup> can provide an accurate measurement of  $\text{pH}_t$  in nearshore waters when SeaFET<sup>TM</sup>  
580 operation is executed with high precision.

581

582 SeaFETs<sup>TM</sup><sub>397, 268</sub> deployed at the APSH and at Sentry Shoal displayed the lowest  
583 uncertainty and greatest precision of  $\text{pH}_t$  measurements (Fig. 2 and 8). In both instances, the  
584 SeaFETs<sup>TM</sup><sub>397, 268</sub> were adequately conditioned (i.e., subjected to *in situ* conditions for ~50 days)  
585 before calibration was performed. The greater overall accuracy displayed by the SeaFET<sup>TM</sup><sub>268</sub> at  
586 Sentry Shoal may be due to the fact that the sensor was exposed to *in situ* conditions for a longer  
587 period of time and re-calibrated multiple times to the same environment. Further, calibration and  
588 reference sample  $\text{pH}_t$  was derived from  $\text{TCO}_2$  and  $p\text{CO}_2$  processed by the BoL at Sentry Shoal  
589 and from  $p\text{CO}_2$  (also measured by BoL) and the TA-salinity relationship (Evans et al. 2015) at  
590 the APSH. It is unclear as to why the sensor accuracy of both Kasitsna Bay SeaFETs<sup>TM</sup><sub>395, 396</sub>

591 was substantially less than the SeaFETs<sup>TM</sup><sub>397, 268</sub> at the APSH or Sentry Shoal. A potential reason  
592 for the low accuracy may be that sensors were calibrated at a reference point that was extreme  
593 relative to the time series pH<sub>t</sub> signal—that is, calibrated at a time of high variability. In this case,  
594 performing an *in situ* multiple-point calibration could have reduced the uncertainty and increased  
595 the accuracy. While previous studies have found that collection and preservation of calibration  
596 and reference samples can result in a decrease in accuracy depending on operator experience  
597 (McLaughlin et al., 2017), the operator in this study was considered to have substantial  
598 experience conducting such operations used in this evaluation. In addition, given the increased  
599 pH<sub>t</sub> variability over a short temporal period—which can be seen at the end of the Kasitsna Bay  
600 deployment (Fig. 4 and 5)—and the low discrepancy between duplicate reference samples, the  
601 former reasoning (i.e., calibrated to an extreme reference point) is a more reasonable explanation  
602 for the reduced accuracy by the Kasitsna Bay SeaFETs<sup>TM</sup><sub>395, 396</sub> than operator experience. We re-  
603 iterate here that reference sample temperature and salinity were used to calculate SeaFET<sup>TM</sup> pH<sub>t</sub>  
604 at the time points in which sensor pH<sub>t</sub> and reference sample pH<sub>t</sub> were compared, thus salinity  
605 was not a confounding factor.

606  
607 Despite the lower accuracy of the Kasitsna Bay SeaFETs<sup>TM</sup><sub>395, 396</sub>, the two sensors  
608 provided a better insight of inter-sensor variability for non-conditioned to the environment and  
609 conditioned electrodes. After *in situ* single-point calibration for conditioned sensors, the average  
610 inter-sensor variability decreased for the internal electrode by ~80%, and >300% for the external  
611 electrode (Fig. 6). The inter-sensor variability reported here was still greater than previous  
612 findings (Kapsenberg et al., 2017), however, the comparison made in this study was done in the  
613 field compared to controlled laboratory conditions as in Kapsenberg et al. (2017). And while  
614 non-homogenized water could lead to anomalies in pH<sub>t</sub> measurements by the Kasitsna Bay  
615 SeaFETs<sup>TM</sup><sub>395, 396</sub>, it is unlikely that water was consistently non-homogenized over the entirety of  
616 a deployment at a distance of < 20 cm (distance between electrodes on each SeaFET<sup>TM</sup>).  
617 Furthermore, due to the dynamic nature of Kachemak Bay, where the tidal exchanges are  
618 extreme, averaging 4.73 m, it is unlikely that micro-heterogeneity of seawater is the driving force  
619 behind the observed differences in pH<sub>t</sub> measurements that were observed between SeaFETs<sup>TM</sup><sub>395,</sub>  
620 <sub>396</sub>. There was a tradeoff for a decrease in inter-sensor variability, as the *in situ* single-point  
621 calibration performed after sensors were conditioned resulted in a decrease in accuracy compared  
622 to an *in situ* single-point calibration performed for sensors not conditioned to the environment. It  
623 should be noted that we do not consider salinity to be a potential source of uncertainty for inter-  
624 sensor variability because the pH<sub>t</sub> difference using data sonde salinity compared to a fixed  
625 salinity resulted in an anomaly of < 0.005 units.

626  
627 The influence of rapid environmental variability should be acknowledged here as this can  
628 create uncertainty in autonomous sensor operation and accuracy (Tamburri et al. 2011).  
629 While the temperature changes due to rapid environmental change in Kasitsna Bay equate to a  
630 potential 0.011 discrepancy in pH, previous evaluation of these sensors show that rapid response  
631 to temperature changes should be negligible and result in uncertainties below the accuracy  
632 assured when applying an average temperature coefficient (k<sub>2</sub>), which can result in discrepancies  
633 of <0.015 pH units (Bresnahan et al. 2014). Rapid changes in salinity could also result in  
634 uncertainties regarding SeaFET<sup>TM</sup> accuracy and may be responsible for the noisier signal  
635 observed by the external electrode for the SeaFETs<sup>TM</sup><sub>395, 396</sub> deployed in Kasitsna Bay. The  
636 greatest salinity change within a 3 h period observed in Kasitsna Bay was 3.90. Given that the

637 mean salinity at the deployment site was 31.8, a mismatch in timing here, or lag in response,  
638 could equate to pH changes as great as 0.053 units—although this likely a high estimate as this  
639 was the maximum difference within a 3 h period. It should be noted that rapid salinity changes  
640 would only affect the external electrode as the internal electrode is insensitive to changes in  
641 salinity. Due to the uncertainties that can emerge from rapid environmental variability, we  
642 reiterate the benefits of an operator understanding the deployment site as this will enhance data  
643 collection by the SeaFET™.

644  
645 The Sentry Shoal SeaFET™<sub>268</sub> had the lowest average pH<sub>t</sub> uncertainty for both electrodes  
646 after *in situ* single-point calibration was performed, however, these were still greater than the pH<sub>t</sub>  
647 uncertainty determined using the factory calibration coefficients. This specific example  
648 highlights two possibilities: (1) the role of inter-sensor variability, as this may be a coincidental  
649 case given the uncertainty observed when quantifying inter-sensor variability, and (2) the  
650 influence of variance within a calibration sample set. For the case of SeaFET™<sub>268</sub>, the replicate  
651 calibration samples collected on 19 July 2016 and 2 September 2016 for the first and second  
652 deployments had standard deviations of 0.016 and 0.005 pH<sub>t</sub> units, respectively. When factory  
653 and *in situ* calibrated data produce final pH<sub>t</sub> values in close agreement, it is important to  
654 recognize that the variance in the calibration sample set may contribute to better agreement  
655 between factory calibrated sensor pH<sub>t</sub> data and average discrete sample pH<sub>t</sub> measurements. It  
656 should also be noted that pre-deployment calibration can provide highly accurate measurements  
657 by the Honeywell Durafet (internal electrode), however, matching exact conditions to those at  
658 the field site are necessary (Johnson et al., 2017), and this was not likely the case for the factory  
659 provided calibration coefficients.

660  
661 The evaluation of SeaFET™ performance presented here corroborates and contrasts with  
662 previous studies examining the overall accuracy and precision of pH<sub>t</sub> measurements made by  
663 these oceanographic instruments. While the accuracy of two SeaFETs™<sub>397, 268</sub> fall well within  
664 the range determined from previous studies, the accuracy of SeaFETs™<sub>395, 396</sub> at Kasitsna Bay  
665 lay outside the bounds of what has been reported in the primary literature (Bresnahan et al.,  
666 2014; Gonski et al., 2018; Johnson et al., 2017; Kapsenberg et al., 2017; Martz et al., 2010). For  
667 example, Bresnahan et al. (2014) describes intrinsic Durafet uncertainties less than 0.03 units,  
668 but this varied depending on the validating reference source (e.g., spectrophotometric pH or pH<sup>est</sup>  
669 from O<sub>2</sub>). One reason as to why our the Kasitsna Bay SeaFET's™ uncertainties differed from  
670 Bresnahan et al. (2014) may be due to the fact that calibration was performed ~78 days after  
671 deployment. Thus, we suggest that in a highly dynamic area such as Kasitsna Bay, calibration  
672 should be performed immediately after conditioning. While there is no way to officially conclude  
673 that this could have reduced uncertainty, it is one potential source of discrepancy. Following  
674 current best practices in Bresnahan et al. (2014) may yield robust measurements, however, the  
675 utility of our assessment describes the importance of knowing when to take calibration samples  
676 as a means to decrease uncertainties. Nevertheless, it is relevant to report the potential  
677 uncertainties possible when operating SeaFETs™ as a multitude of factors can influence the  
678 overall accuracy (e.g., operator, sample preservation, electrode conditioning, calibration  
679 measurements), therefore, the potential uncertainties calculated in this study represent the upper  
680 limit of an average uncertainty compiled from four different SeaFETs™ (Fig. 10). The utility of  
681 such an analysis provides a confidence in SeaFET™ operation, and highlights all the potential  
682 uncertainties that need to be considered when deploying the sensors in the field. For example, we

683 have included a thermistor uncertainty term determined from the test tank and field deployments  
684 of the Alaska SeaFETs<sup>TM</sup><sub>395, 396, 397</sub>, even though a suitable solution around this issue would be to  
685 apply an offset to the thermistor temperature given it was compared to more robust temperature  
686 measurements conducted before field deployment. It should be noted, that in this case, the  
687 thermistor uncertainty observed from SeaFET<sup>TM</sup><sub>397</sub> against the BoL was excluded as the lag time  
688 between thermistor response and tank residence time likely confounded the comparison. The  
689 potential pH<sub>t</sub> uncertainties presented here should serve as a guide for SeaFET<sup>TM</sup> operators in  
690 order to better understand the source of an uncertainty and take the necessary steps to improve  
691 SeaFET<sup>TM</sup> measurements. Bresnahan et al. (2014) acknowledged that relying on the SeaFET<sup>TM</sup>  
692 for an accurate pH measurement should be viewed cautiously if additional biogeochemical  
693 sensors are not co-deployed to cross-validate the stability and accuracy of the SeaFET's<sup>TM</sup>  
694 electrodes, therefore, being fully aware of all the potential uncertainties presented here will only  
695 further aid SeaFET<sup>TM</sup> operators.

696  
697 The time series data provided by the SeaFET<sup>TM</sup> deployments in this study have expanded  
698 the extent of recorded pH<sub>t</sub> variability along the North American west coast. The SeaFETs<sup>TM</sup><sub>395,</sub>  
699 <sub>396</sub> deployed in Kasitsna Bay provide some of the first high temporal resolution measurements of  
700 pH<sub>t</sub> in this region. During this spring deployment, it appears that semi-diurnal tidal fluctuations  
701 are the dominant contributor to pH<sub>t</sub> variability with an additional cycle occurring every 21 days  
702 coinciding with the seasonal spring and neap tides (Fig. 9). The SeaFET<sup>TM</sup><sub>268</sub> at Sentry Shoal  
703 also displays a strong pH<sub>t</sub> response to the semi-diurnal mixed tidal cycle. A strong signal is also  
704 present at a frequency of zero, and is likely a result of the long, across-season, time series. That  
705 is, over the course of the entire deployment which went from summer into late fall, seasonal  
706 drivers of pH<sub>t</sub> (e.g., decrease in water temperature) confounded repetitive frequency patterns. In  
707 addition, Sentry Shoal may have a weaker tidal signature relative to other pH<sub>t</sub> modulators that do  
708 not follow a cyclical pattern such as water mass intrusion, inconsistent metabolic cycles from the  
709 end of summer into the fall season, and a shift to the rainy season.

710  
711 As an elaboration on the power spectral density analysis, we suggest this form of  
712 frequency analysis can be utilized to better understand the system in which a SeaFET<sup>TM</sup> is  
713 deployed, thus informing the operator as to what the drivers of their system are, and when to  
714 calibrate the sensor. It is possible that in a highly dynamic setting, the sensor could re-condition  
715 over time periods not resolved in a multi-point calibration sampling scheme, and this could  
716 enhance sensor inaccuracies. For example, in Kasitsna Bay, a strong semi-diurnal tide cycle was  
717 present, so upon redeployment in this area, if possible, the best calibration approach would be an  
718 *in situ* multi-point calibration between the mixed semi-diurnal tidal cycle. Alternatively, if the  
719 system is not driven by a strong tidal signature (e.g., non-coastal region), an *in situ* single-point  
720 calibration may be a reasonable approach. It should be noted that while spectral analysis can be  
721 used as an additional tool to better calibrate the SeaFET<sup>TM</sup>, specific coastal environments with  
722 dynamic storm frequencies or varying photosynthesis and respiration cycles could obscure a  
723 clear driving frequency of pH change. In these situations, capturing the dynamic range (i.e.,  
724 multiple calibration samples over this period) of one of these events may be sufficient to provide  
725 best approach for robust calibration.

## 726 727 **5 Conclusion**

728



729 The following evaluation of the Sea-Bird SeaFET™ helped elucidate the overall  
730 accuracy and highlighted the potential uncertainties and pitfalls of operating and obtaining pH<sub>t</sub>  
731 measurements by the internal and external electrode pair. We found that the internal electrode  
732 provided the more robust measurement in nearshore estuarine waters when an *in situ* multi-point  
733 calibration was performed (Fig. 10). The quantified potential pH<sub>t</sub> uncertainty is based  
734 specifically on our findings, whereas further results may minimize this uncertainty given  
735 additional evaluations. However, the results here provide an upper limit of the pH<sub>t</sub> uncertainty  
736 that may be observed when operating a Sea-Bird SeaFET™. Further, high temporal resolution  
737 pH<sub>t</sub> measurements in nearshore Canadian and Alaskan waters provide a better understanding of  
738 the drivers modulating pH on short timescales. Given the application, the Sea-Bird SeaFET™  
739 can provide a reliable and accurate pH<sub>t</sub> measurement which can be utilized to broaden the  
740 coverage of understanding pH variability in nearshore and open-ocean waters.

741

## 742 **Acknowledgments**

743 The authors would like to thank Jeff Hetrick and Jacqueline Ramsey at the Alutiiq Pride  
744 Shellfish Hatchery for providing their facilities and services for this evaluation. We would also  
745 like to thank Angela Doroff at the Kasitsna Bay laboratory for providing facilities for SeaFET™  
746 deployments. Funding for this project was provided in part by the University of Alaska  
747 Fairbanks College of Fisheries and Ocean Sciences. WE and KP thank the Pacific Salmon  
748 Foundation and Environment Canada for providing the platform for deploying SeaFET 268, the  
749 University of Alaska Fairbanks Ocean Acidification Research Center for the long-term use of  
750 SeaFET 268, and the Tula Foundation for supporting their efforts with this work.

751

752

## 753 **References**

- 754 Bandstra, L., Hales, B. and Takahashi, T.: High-frequency measurements of total CO<sub>2</sub>: Method  
755 development and first oceanographic observations, *Mar. Chem.*, 100(1–2), 24–38,  
756 doi:10.1016/j.marchem.2005.10.009, 2006.
- 757 Barton, A., Hales, B., Waldbusser, G. G., Langdon, C. and Feely, R. A.: The Pacific oyster,  
758 *Crassostrea gigas*, shows negative correlation to naturally elevated carbon dioxide levels:  
759 Implications for near-term ocean acidification effects, *Limnol. Oceanogr.*, 57(3), 698–710,  
760 doi:10.4319/lo.2012.57.3.0698, 2012.
- 761 Bresnahan, P. J., Martz, T. R., Takeshita, Y., Johnson, K. S. and LaShomb, M.: Best practices for  
762 autonomous measurement of seawater pH with the Honeywell Durafet, *Methods Oceanogr.*, 9,  
763 44–60, doi:10.1016/j.mio.2014.08.003, 2014.
- 764 Caldeira, K. and Wickett, M. E.: Anthropogenic carbon and ocean pH, *Nature*, 425(6956), 365–  
765 365, doi:10.1038/425365a, 2003.
- 766 Chan, F., Barth, J. A., Blanchette, C. A., Byrne, R. H., Chavez, F., Cheriton, O., Feely, R. A.,  
767 Friederich, G., Gaylord, B., Gouhier, T., Hacker, S., Hill, T., Hofmann, G., McManus, M. A.,  
768 Menge, B. A., Nielsen, K. J., Russell, A., Sanford, E., Sevadjan, J. and Washburn, L.: Persistent  
769 spatial structuring of coastal ocean acidification in the California Current System, *Sci. Rep.*, 7(1),  
770 2526, doi:10.1038/s41598-017-02777-y, 2017.

771 Dickson, A. G., Sabine, C. L. and Christian, J. R.: Guide to Best Practices for Ocean CO<sub>2</sub>  
772 Measurements., Report, North Pacific Marine Science Organization. [online] Available from:  
773 <http://www.oceandatapactices.net:80/handle/11329/249>, 2007.

774 Duarte, C. M., Hendriks, I. E., Moore, T. S., Olsen, Y. S., Steckbauer, A., Ramajo, L.,  
775 Carstensen, J., Trotter, J. A. and McCulloch, M.: Is Ocean Acidification an Open-Ocean  
776 Syndrome? Understanding Anthropogenic Impacts on Seawater pH, *Estuaries Coasts*, 36(2),  
777 221–236, doi:10.1007/s12237-013-9594-3, 2013.

778 Ekstrom, J. A., Suatoni, L., Cooley, S. R., Pendleton, L. H., Waldbusser, G. G., Cinner, J. E.,  
779 Ritter, J., Langdon, C., van Hooidek, R., Gledhill, D., Wellman, K., Beck, M. W., Brander, L.  
780 M., Rittschof, D., Doherty, C., Edwards, P. E. T. and Portela, R.: Vulnerability and adaptation of  
781 US shellfisheries to ocean acidification, *Nat. Clim. Change*, 5(3), 207–214,  
782 doi:10.1038/NCLIMATE2508, 2015.

783 Evans, W., Mathis, J. T. and Cross, J. N.: Calcium carbonate corrosivity in an Alaskan inland  
784 sea, *Biogeosciences*, 11(2), 365–379, doi:10.5194/bg-11-365-2014, 2014.

785 Evans, W., Mathis, J. T., Ramsay, J. and Hetrick, J.: On the Frontline: Tracking Ocean  
786 Acidification in an Alaskan Shellfish Hatchery, *PLOS ONE*, 10(7), e0130384,  
787 doi:10.1371/journal.pone.0130384, 2015.

788 Feely, R. A., Alin, S. R., Newton, J., Sabine, C. L., Warner, M., Devol, A., Krembs, C. and  
789 Maloy, C.: The combined effects of ocean acidification, mixing, and respiration on pH and  
790 carbonate saturation in an urbanized estuary, *Estuar. Coast. Shelf Sci.*, 88(4), 442–449,  
791 doi:10.1016/j.ecss.2010.05.004, 2010.

792 Feely, R. A., Alin, S. R., Carter, B., Bednaršek, N., Hales, B., Chan, F., Hill, T. M., Gaylord, B.,  
793 Sanford, E., Byrne, R. H., Sabine, C. L., Greeley, D. and Juranek, L.: Chemical and biological  
794 impacts of ocean acidification along the west coast of North America, *Estuar. Coast. Shelf Sci.*,  
795 183, Part A, 260–270, doi:10.1016/j.ecss.2016.08.043, 2016.

796 Gonski, S. F., Cai, W.-J., Ullman, W. J., Joesoef, A., Main, C. R., Pettay, D. T. and Martz, T. R.:  
797 Assessment of the suitability of Durafet-based sensors for pH measurement in dynamic estuarine  
798 environments, *Estuar. Coast. Shelf Sci.*, 200(Supplement C), 152–168,  
799 doi:10.1016/j.ecss.2017.10.020, 2018.

800 Hales, B., Suhrbier, A., Waldbusser, G. G., Feely, R. A. and Newton, J. A.: The Carbonate  
801 Chemistry of the “Fattening Line,” Willapa Bay, 2011–2014, *Estuaries Coasts*, 1–14,  
802 doi:10.1007/s12237-016-0136-7, 2016.

803 Harris, K. E., DeGrandpre, M. D. and Hales, B.: Aragonite saturation state dynamics in a coastal  
804 upwelling zone, *Geophys. Res. Lett.*, 40(11), 2720–2725, doi:10.1002/grl.50460, 2013.

805 Hofmann, G. E., Smith, J. E., Johnson, K. S., Send, U., Levin, L. A., Micheli, F., Paytan, A.,  
806 Price, N. N., Peterson, B., Takeshita, Y., Matson, P. G., Crook, E. D., Kroeker, K. J., Gambi, M.  
807 C., Rivest, E. B., Frieder, C. A., Yu, P. C. and Martz, T. R.: High-Frequency Dynamics of Ocean

808 pH: A Multi-Ecosystem Comparison, *Plos One*, 6(12), e28983,  
809 doi:10.1371/journal.pone.0028983, 2011.

810 Johnson, K. S., Plant, J. N., Coletti, L. J., Jannasch, H. W., Sakamoto, C. M., Riser, S. C., Swift,  
811 D. D., Williams, N. L., Boss, E., Haentjens, N., Talley, L. D. and Sarmiento, J. L.:  
812 Biogeochemical sensor performance in the SOCCOM profiling float array, *J. Geophys. Res.-*  
813 *Oceans*, 122(8), 6416–6436, doi:10.1002/2017JC012838, 2017.

814 Kapsenberg, L., Bockmon, E. E., Bresnahan, P. J., Kroeker, K. J., Gattuso, J.-P. and Martz, T.  
815 R.: Advancing Ocean Acidification Biology Using Durafet® pH Electrodes, *Front. Mar. Sci.*, 4,  
816 doi:10.3389/fmars.2017.00321, 2017.

817 Kapsenberg, L. and Hofmann, G. E.: Ocean pH time-series and drivers of variability along the  
818 northern Channel Islands, California, USA, *Limnol. Oceanogr.*, 61(3), 953–968,  
819 doi:10.1002/lno.10264, 2016.

820 Kapsenberg, L., Kelley, A. L., Shaw, E. C., Martz, T. R. and Hofmann, G. E.: Near-shore  
821 Antarctic pH variability has implications for the design of ocean acidification experiments, *Sci.*  
822 *Rep.*, 5, srep09638, doi:10.1038/srep09638, 2015.

823 Khoo, K. H., Ramette, R. W., Culbertson, C. H. and Bates, R. G.: Determination of hydrogen ion  
824 concentrations in seawater from 5 to 40.degree.C: standard potentials at salinities from 20 to  
825 45%, *Anal. Chem.*, 49(1), 29–34, doi:10.1021/ac50009a016, 1977.

826 Lueker, T. J., Dickson, A. G. and Keeling, C. D.: Ocean pCO<sub>2</sub> calculated from dissolved  
827 inorganic carbon, alkalinity, and equations for K-1 and K-2: validation based on laboratory  
828 measurements of CO<sub>2</sub> in gas and seawater at equilibrium, *Mar. Chem.*, 70(1–3), 105–119,  
829 doi:10.1016/S0304-4203(00)00022-0, 2000.

830 Martz, T., Send, U., Ohman, M. D., Takeshita, Y., Bresnahan, P., Kim, H.-J. and Nam, S.:  
831 Dynamic variability of biogeochemical ratios in the Southern California Current System,  
832 *Geophys. Res. Lett.*, 41(7), 2496–2501, doi:10.1002/2014GL059332, 2014.

833 Martz, T. R., Connery, J. G. and Johnson, K. S.: Testing the Honeywell Durafet® for seawater  
834 pH applications, *Limnol. Oceanogr. Methods*, 8(5), 172–184, doi:10.4319/lom.2010.8.172, 2010.

835 Martz, T. R., Daly, K. L., Byrne, R. H., Stillman, J. H. and Turk, D.: Technology for ocean  
836 acidification research: needs and availability, *Oceanography*, 28(2), 40–47, 2015.

837 Mathis, J. T., Cross, J. N. and Bates, N. R.: Coupling primary production and terrestrial runoff to  
838 ocean acidification and carbonate mineral suppression in the eastern Bering Sea, *J. Geophys.*  
839 *Res. Oceans*, 116(C2), C02030, doi:10.1029/2010JC006453, 2011a.

840 Mathis, J. T., Cross, J. N. and Bates, N. R.: The role of ocean acidification in systemic carbonate  
841 mineral suppression in the Bering Sea, *Geophys. Res. Lett.*, 38(19), L19602,  
842 doi:10.1029/2011GL048884, 2011b.

843 Mathis, J. T., Pickart, R. S., Byrne, R. H., McNeil, C. L., Moore, G. W. K., Juranek, L. W., Liu,  
844 X., Ma, J., Easley, R. A., Elliot, M. M., Cross, J. N., Reisdorph, S. C., Bahr, F., Morison, J.,  
845 Lichendorf, T. and Feely, R. A.: Storm-induced upwelling of high pCO<sub>2</sub> waters onto the  
846 continental shelf of the western Arctic Ocean and implications for carbonate mineral saturation  
847 states, *Geophys. Res. Lett.*, 39(7), L07606, doi:10.1029/2012GL051574, 2012.

848 Mathis, J. T., Cross, J. N., Monacci, N., Feely, R. A. and Stabeno, P.: Evidence of prolonged  
849 aragonite undersaturations in the bottom waters of the southern Bering Sea shelf from  
850 autonomous sensors, *Deep-Sea Res. Part II-Top. Stud. Oceanogr.*, 109, 125–133,  
851 doi:10.1016/j.dsr2.2013.07.019, 2014.

852 Mathis, J. T., Cross, J. N., Evans, W. and Doney, S. C.: Ocean Acidification in the Surface  
853 Waters of the Pacific-Arctic Boundary Regions, *Oceanography*, 28(2), 122–135,  
854 doi:10.5670/oceanog.2015.36, 2015a.

855 Mathis, J. T., Cooley, S. R., Lucey, N., Colt, S., Ekstrom, J., Hurst, T., Hauri, C., Evans, W.,  
856 Cross, J. N. and Feely, R. A.: Ocean acidification risk assessment for Alaska’s fishery sector,  
857 *Prog. Oceanogr.*, 136, 71–91, doi:10.1016/j.pocean.2014.07.001, 2015b.

858 Matson, P. G., Martz, T. R. and Hofmann, G. E.: High-frequency observations of pH under  
859 Antarctic sea ice in the southern Ross Sea, *Antarct. Sci.*, 23(6), 607–613,  
860 doi:10.1017/S0954102011000551, 2011.

861 McLaughlin, K., Dickson, A., Weisberg, S. B., Coale, K., Elrod, V., Hunter, C., Johnson, K. S.,  
862 Kram, S., Kudela, R., Martz, T., Negrey, K., Passow, U., Shaughnessy, F., Smith, J. E., Tadesse,  
863 D., Washburn, L. and Weis, K. R.: An evaluation of ISFET sensors for coastal pH monitoring  
864 applications, *Reg. Stud. Mar. Sci.*, 12, 11–18, doi:10.1016/j.rsma.2017.02.008, 2017.

865 Newton J.A., Feely R. A., Jewett E. B., Williamson P. & Mathis J.  
866 2015. Global Ocean Acidification Observing Network: Requirements and Governance Plan.  
867 Second Edition, GOA-ON, [http://www.goa-on.org/docs/GOA-ON\\_plan\\_print.pdf](http://www.goa-on.org/docs/GOA-ON_plan_print.pdf).  
868

869 Newton, J., Devol, A., Alford, M., Mickett, J., Sabine, C. and Sutton, A.: Nanoos Contributions  
870 to Understanding Ocean Acidification, *J. Shellfish Res.*, 31(1), 327–327, 2012.

871 Orr, J. C., Fabry, V. J., Aumont, O., Bopp, L., Doney, S. C., Feely, R. A., Gnanadesikan, A.,  
872 Gruber, N., Ishida, A., Joos, F., Key, R. M., Lindsay, K., Maier-Reimer, E., Matear, R., Monfray,  
873 P., Mouchet, A., Najjar, R. G., Plattner, G. K., Rodgers, K. B., Sabine, C. L., Sarmiento, J. L.,  
874 Schlitzer, R., Slater, R. D., Totterdell, I. J., Weirig, M. F., Yamanaka, Y. and Yool, A.:  
875 Anthropogenic ocean acidification over the twenty-first century and its impact on calcifying  
876 organisms, *Nature*, 437(7059), 681–686, doi:10.1038/nature04095, 2005.

877 Orr, J. C., J.-M. Epitalon, A. G. Dickson, and J.-P. Gattuso: Routine uncertainty propagation for  
878 the marine carbon dioxide system, *Marine Chemistry*, *in prep.*  
879

880 Riebesell, U. and Gattuso, J.-P.: Lessons learned from ocean acidification research, *Nat. Clim.*  
881 *Change*, 5(1), 12–14, doi:10.1038/nclimate2456, 2015.

882 Rudd, M. A.: What a Decade (2006–15) Of Journal Abstracts Can Tell Us about Trends in  
883 Ocean and Coastal Sustainability Challenges and Solutions, *Front. Mar. Sci.*, 4,  
884 doi:10.3389/fmars.2017.00170, 2017.

885 Steinhart, J. S. and Hart, S. R.: Calibration curves for thermistors, *Deep Sea Res. Oceanogr.*  
886 *Abstr.*, 15(4), 497–503, doi:10.1016/0011-7471(68)90057-0, 1968.

887 Sunda, W. G. and Cai, W.-J.: Eutrophication Induced CO<sub>2</sub>-Acidification of Subsurface Coastal  
888 Waters: Interactive Effects of Temperature, Salinity, and Atmospheric P-CO<sub>2</sub>, *Environ. Sci.*  
889 *Technol.*, 46(19), 10651–10659, doi:10.1021/es300626f, 2012.

890 Takeshita, Y., Martz, T. R., Johnson, K. S. and Dickson, A. G.: Characterization of an Ion  
891 Sensitive Field Effect Transistor and Chloride Ion Selective Electrodes for pH Measurements in  
892 Seawater, *Anal. Chem.*, 86(22), 11189–11195, doi:10.1021/ac502631z, 2014.

893• Tamburri, M. N., Johengen, T. H., Atkinson, M. J., Schar, D. W. H., Robertson, C. Y., Purcell,  
894 H., Smith, G. J., Pinchuk, A. and Buckley, E. N.: Alliance for Coastal Technologies, *Marine*  
895 *Technology Society Journal*, 45(1), 43–51, doi: 10.4031/MTSJ.45.1.4, 2011.

896 Uppström, L. R.: The boron/chlorinity ratio of deep-sea water from the Pacific Ocean, *Deep Sea*  
897 *Res. Oceanogr. Abstr.*, 21, 161–162, doi:10.1016/0011-7471(74)90074-6, 1974.

898 Waldbusser, G. G. and Salisbury, J. E.: Ocean Acidification in the Coastal Zone from an  
899 Organism's Perspective: Multiple System Parameters, Frequency Domains, and Habitats,  
900 *Annu. Rev. Mar. Sci.*, 6(1), 221–247, doi:10.1146/annurev-marine-121211-172238, 2014.

901 Yu, P. C., Matson, P. G., Martz, T. R. and Hofmann, G. E.: The ocean acidification seascape and  
902 its relationship to the performance of calcifying marine invertebrates: Laboratory experiments on  
903 the development of urchin larvae framed by environmentally-relevant pCO<sub>2</sub>/pH, *J. Exp. Mar.*  
904 *Biol. Ecol.*, 400(1–2), 288–295, doi:10.1016/j.jembe.2011.02.016, 2011.

905  
906  
907  
908  
909  
910  
911  
912  
913  
914  
915  
916  
917  
918  
919  
920

921 **Table 1.** Deployment regime of all four SeaFETs™ including deployment location, date, and  
 922 calibration methods performed. \*Non-controlled source water pumped directly from  
 923 Resurrection Bay, AK, USA.  
 924

Location (Tank or Field)	Date	SeaFET™ ID	Average reads frame <sup>-1</sup>	Frames Burst <sup>-1</sup>	Sampling Freq. (min)	Calibration method
APSH — <i>Tank</i>	5 – 8 October 2016	395, 396, 397	1	10	5	Factory
OARC — <i>Tank</i>	26 October – 3 November 2016	395, 396, 397	3	—	Continuous	Factory
OARC — <i>Tank</i>	26 January – 1 February 2017	395, 396, 397	1	10	180	Factory
APSH <i>Field*</i>	5 March – 6 June 2017	397	10	30	180	Factory, SP and MP <i>in situ</i>
Kachemak Bay <i>Field</i>	18 March – 4 June 2017	395, 396	10	30	180	Factory, SP <i>in situ</i>
Sentry Shoal <i>Field</i>	6 July – 23 August, 27 August – 28 November 2016	268	10	30	30	Factory, SP <i>in situ</i>

925  
 926  
 927 Factory: factory calibration; SP: *in situ* single-point calibration; MP: *in situ* multi-point  
 928 calibration.  
 929  
 930  
 931  
 932  
 933  
 934  
 935  
 936  
 937  
 938  
 939  
 940  
 941  
 942  
 943  
 944  
 945  
 946  
 947  
 948  
 949  
 950

951 **Table 2.** Terms and definitions used to describe the evaluation of the Sea-Bird SeaFET™ based  
 952 on observations specific to this study.

953  
 954

Terms	Definiiton
Uncertainty	One or multiple factors that result in a discrepancy between SeaFET™ pH - "True pH" that are non-correctable
Accuracy	Difference between SeaFET™ pH - "True pH"
Overall Accuracy	Integrated uncertainties
"True pH <sub>t</sub> "	pH on the total scale measured by robust bench top methods: either VINDTA 3C or the Burke-o-lator
Variability	Specific difference in pH <sub>t</sub> between the internal or external electrodes on SeaFETs™ 395 and 396
Mean Anomaly	Average difference between the internal and external electrode pH <sub>t</sub>

955  
 956  
 957  
 958  
 959  
 960  
 961  
 962  
 963  
 964  
 965  
 966  
 967  
 968  
 969  
 970  
 971  
 972  
 973  
 974  
 975  
 976  
 977  
 978  
 979

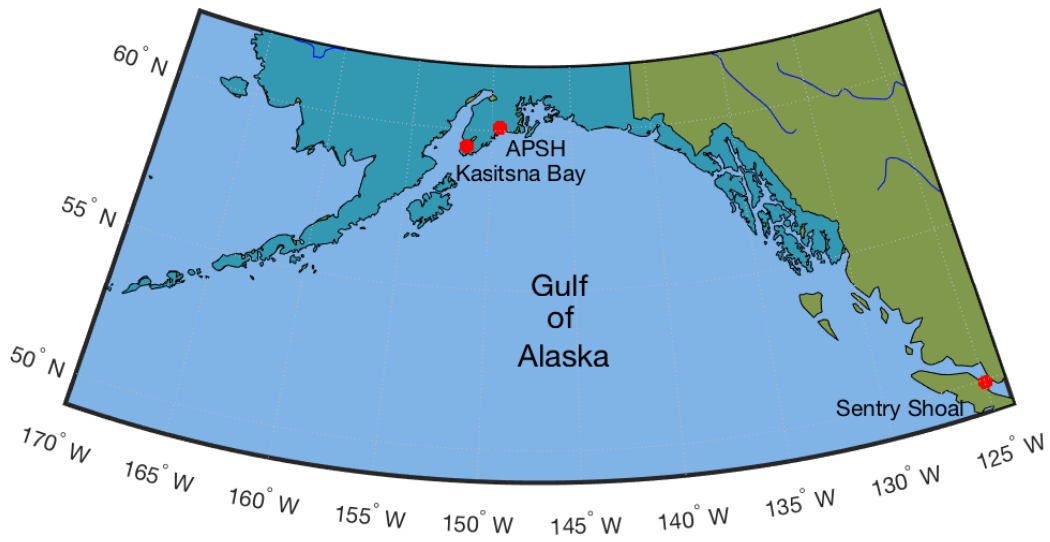
980 **Table 3.** One-way Analysis of variance comparing the  $pH_t$  error (SeaFET™  $pH_t$  – BoL  $pH_t$ )  
 981 across calibration methods for both the internal and external electrodes onboard SeaFETs™<sub>268</sub> at  
 982 Sentry Shoal (factory calibration and *in situ* single-point calibration) and SeaFET™<sub>397</sub> at the  
 983 Alutiiq Pride Shellfish Hatchery (factory calibration, *in situ* single-point calibration, and *in situ*  
 984 multi-point calibration). Bold type denotes statistical significance.  
 985

Site	Electrode	Source	SS	df	MS	F	p-value
APSH	Internal	Fac Cal. Vs. Single-point	27.5	1	27.5	4.96E+04	< <b>0.001</b>
		Error	0.225	406	0.001		
		Total	27.7	407			
APSH	External	Fac Cal. Vs. Single-point	0.681	1	0.681	536	< <b>0.001</b>
		Error	0.516	406	0.001		
		Total	1.19	407			
APSH	Internal	Factory Cal. vs. Multi-point	28.3	1	28.3	6.19E+04	< <b>0.001</b>
		Error	0.185	406	0.001		
		Total	28.5	407			
APSH	External	Factory Cal. vs. Multi-point	0.692	1	0.692	539	< <b>0.001</b>
		Error	0.521	406	0.001		
		Total	1.21	407			
APSH	Internal	Single-point vs. Multi-point	0.005	1	0.005	15.0	< <b>0.001</b>
		Error	0.143	406	0.000		
		Total	0.148	407			
APSH	External	Single-point vs. Multi-point	0.000	1	0.000	0.040	0.843
		Error	0.415	406	0.001		
		Total	0.415	407			

986  
 987  
 988  
 989  
 990  
 991  
 992  
 993  
 994  
 995  
 996  
 997  
 998  
 999  
 1000  
 1001  
 1002  
 1003  
 1004  
 1005  
 1006  
 1007  
 1008  
 1009



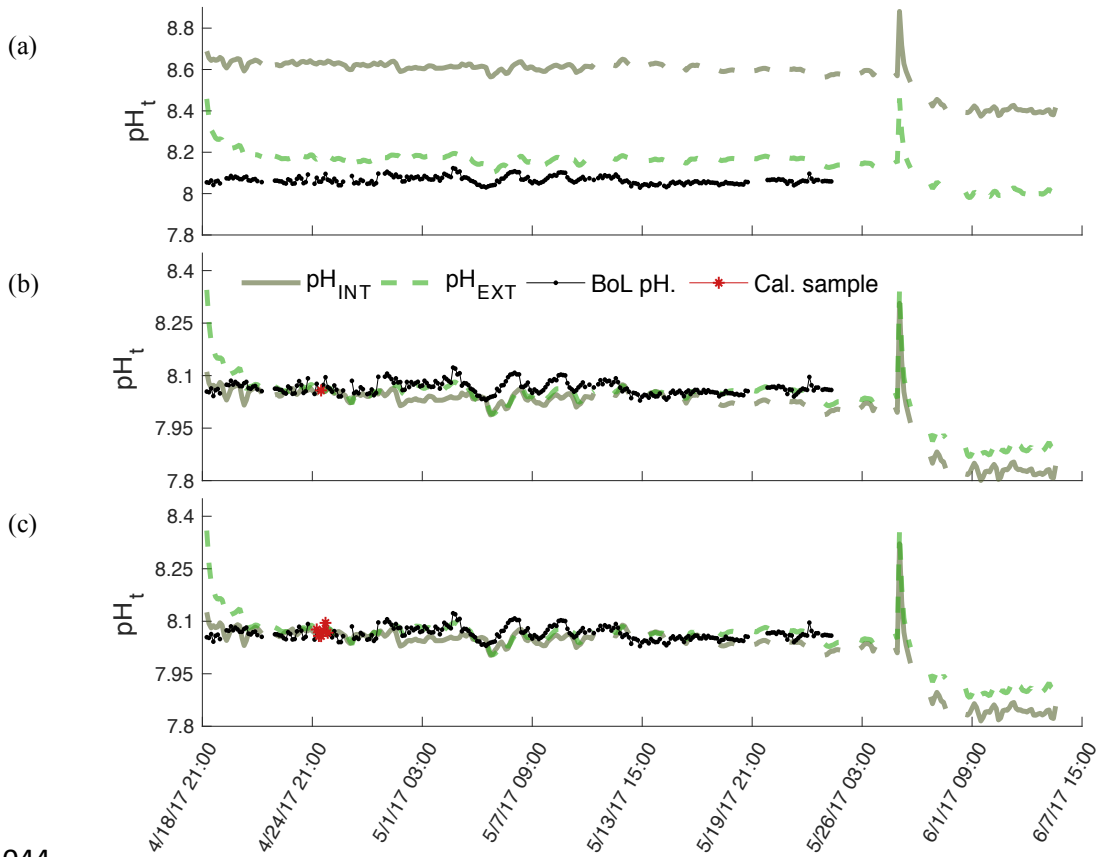
1010 **Figure 1.**  
1011  
1012



1013  
1014  
1015 Geographical map with locations of SeaFET™ field deployments along Alaska's, USA, south-  
1016 central coast and one location in the Strait of Georgia, British Columbia, Canada.

1017  
1018  
1019  
1020  
1021  
1022  
1023  
1024  
1025  
1026  
1027  
1028  
1029  
1030  
1031  
1032  
1033  
1034  
1035  
1036  
1037  
1038  
1039  
1040  
1041

1042 **Figure 2.**  
 1043

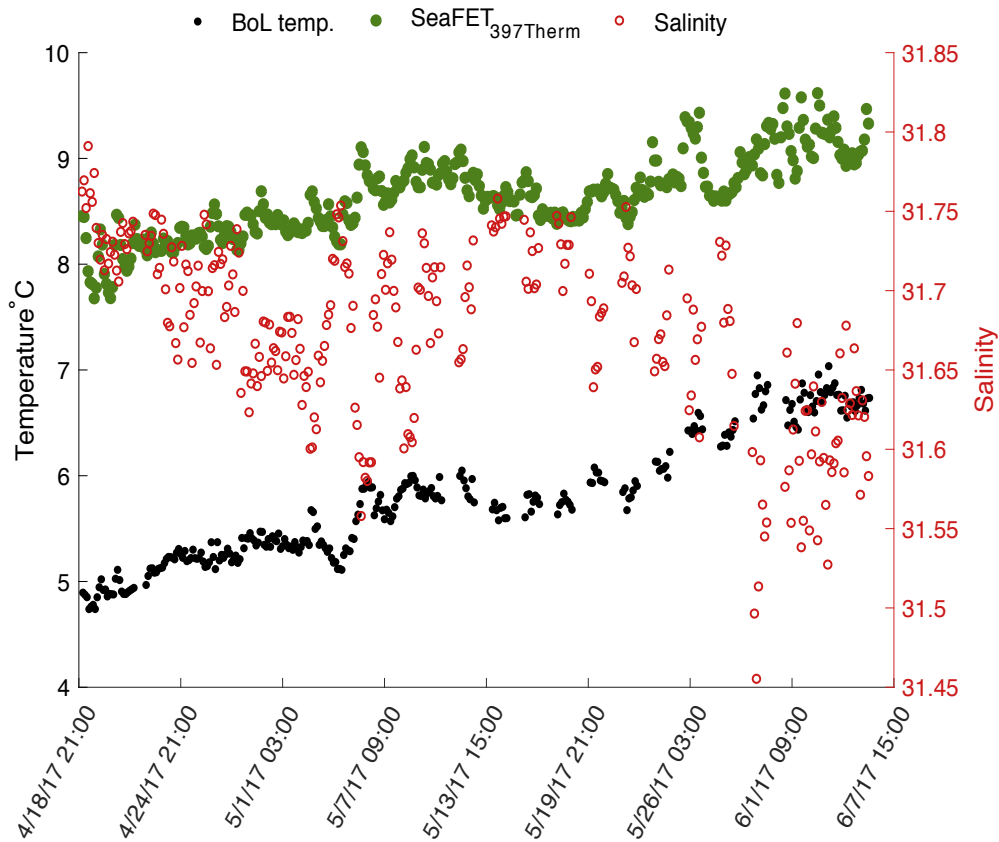


1044  
 1045

1046  $pH_t$  recorded by the internal (solid) and external (dashed) electrodes on SeaFET<sup>TM</sup><sub>397</sub> deployed in  
 1047 parallel with the BoL at the Alutiiq Pride Shellfish Hatchery.  $pH_t$  from both electrodes is shown  
 1048 when derived using factory calibration (FC) coefficients (panel a), *in situ* single-point (SC)  
 1049 calibration coefficients (panel b), and *in situ* multi-point (MC) calibration coefficients (panel c).  
 1050 Black solid line is  $pH_t$  derived from continuous  $pCO_2$  measurements recorded by the BoL and  
 1051 derived TA from the TA-S relationship (Evans et al. 2015). Red circles are the calibration points  
 1052 from the BoL data.

1053  
 1054  
 1055  
 1056  
 1057  
 1058  
 1059  
 1060  
 1061  
 1062  
 1063  
 1064  
 1065

1066 **Figure 3.**  
1067



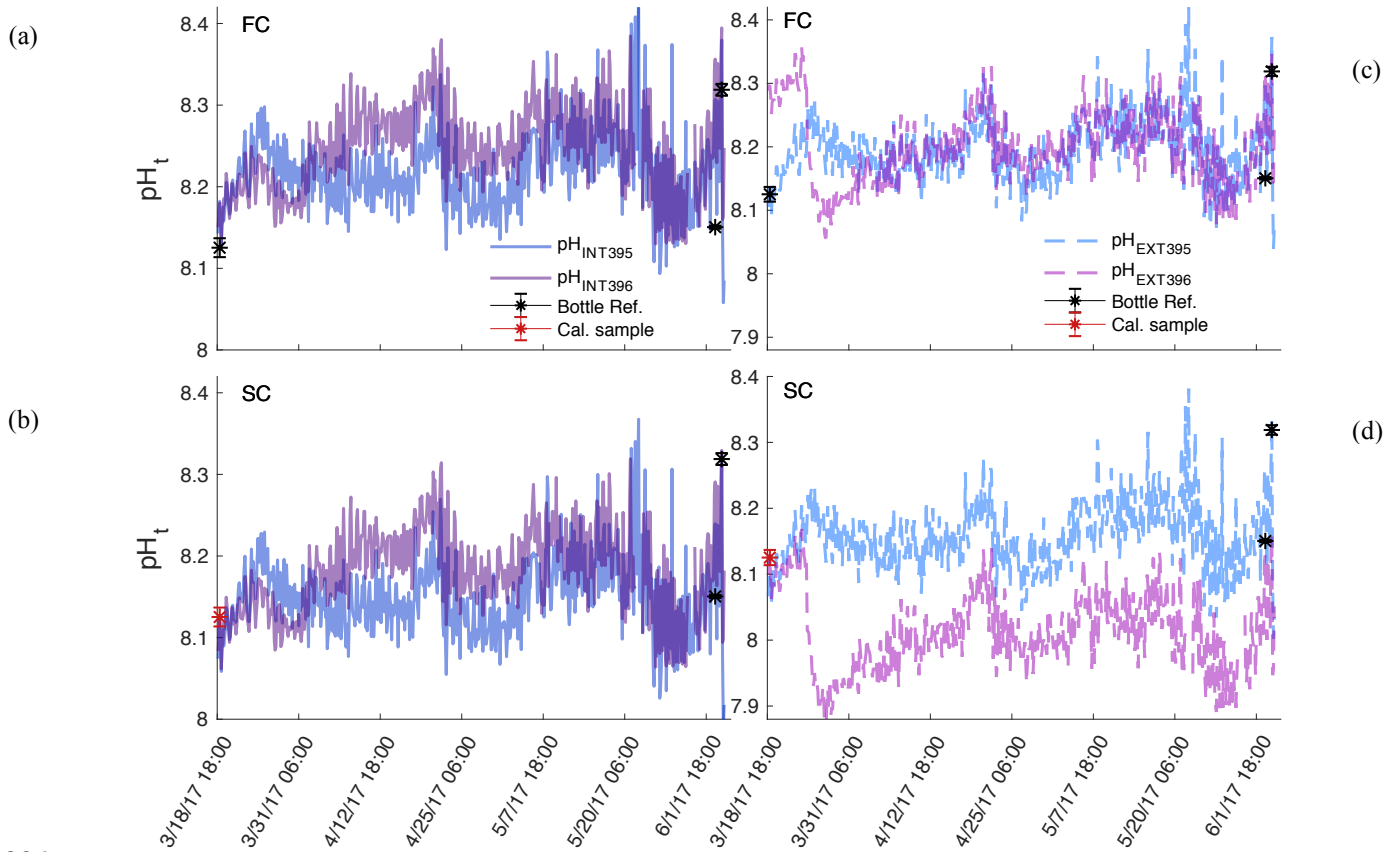
1068  
1069

1070 Temperature derived from the internal thermistor on SeaFET<sup>TM</sup><sub>397</sub> (green circles) and the  
1071 temperature recorded by the BoL (black circles) at the Alutiiq Pride Shellfish Hatchery from late  
1072 winter through spring 2017. Salinity (red circles) recorded by the BoL on the right y-axis.  
1073 SeaFET<sup>TM</sup><sub>397</sub> was only partially submerged resulting in the top half of the sensor exposed to air  
1074 temperature fluctuations.

1075  
1076  
1077  
1078  
1079  
1080  
1081  
1082  
1083  
1084  
1085  
1086  
1087  
1088  
1089

1090  
1091  
1092  
1093

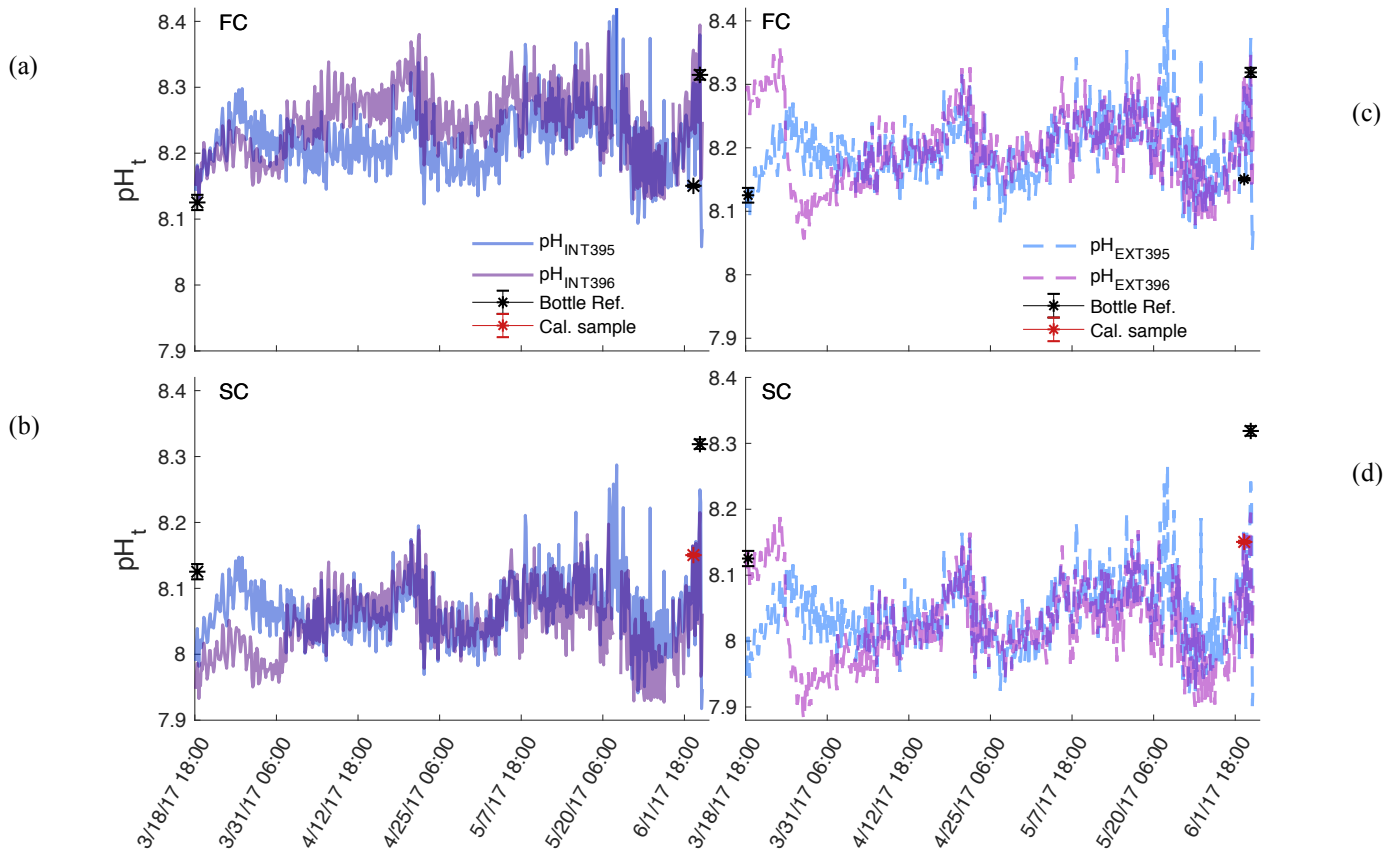
Figure 4.



1094  
1095  
1096  
1097  
1098  
1099  
1100  
1101  
1102  
1103  
1104  
1105  
1106  
1107  
1108  
1109  
1110  
1111  
1112

Comparison of pH<sub>t</sub> recorded by the internal (panel a and b) and external (panel c and d) electrodes on SeaFET<sup>TM</sup><sub>395</sub> (blue) and SeaFET<sup>TM</sup><sub>396</sub> (purple) before they were conditioned to the environment (non-conditioned) deployed in Kasitsna Bay, AK, based on calibration method: factory calibration (FC) and *in situ* single-point (SC) calibration. Discrete reference samples (black asterisks) and calibration sample (red asterisks) were collected 36 and 12 h pre-SeaFET<sup>TM</sup> recovery, and < 24 h post-deployment, respectively. Temperature and salinity measurements collected on reference and calibration samples were used to derive SeaFET<sup>TM</sup> pH<sub>t</sub> at those given time points. All other SeaFET<sup>TM</sup> pH<sub>t</sub> measurements use thermistor temperature and salinity logged by Kasitsna Bay data sonde.

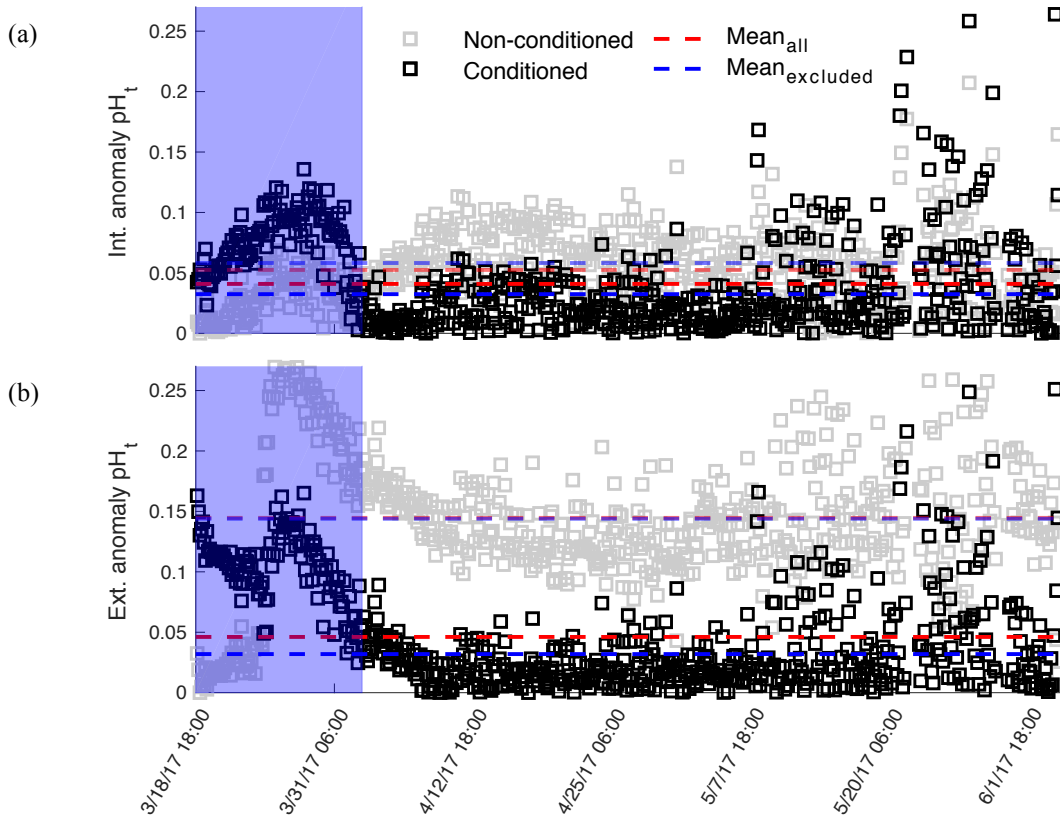
1113 **Figure 5.**  
 1114



1115  
 1116  
 1117 Comparison of  $pH_t$  recorded by the internal (panel a and b) and external (panel c and d)  
 1118 electrodes on conditioned SeaFET<sup>TM</sup><sub>395</sub> (blue) and SeaFET<sup>TM</sup><sub>396</sub> (purple) deployed in Kasitsna  
 1119 Bay, AK, based on calibration method: factory calibration (FC) and *in situ* single-point (SC)  
 1120 calibration. The data set here is the same as figure 4, but timing of calibration method is  
 1121 different. Discrete reference samples (black asterisks) and calibration sample (red asterisks) were  
 1122 collected < 24 h post deployment and 12 h pre-SeaFET<sup>TM</sup> recovery, while calibration sample was  
 1123 collected 36 h pre-SeaFET<sup>TM</sup> recovery. Temperature and salinity measurements collected on  
 1124 reference and calibration samples were used to derive SeaFET<sup>TM</sup>  $pH_t$  at those given time points.  
 1125 All other SeaFET<sup>TM</sup>  $pH_t$  measurements use thermistor temperature and salinity logged by  
 1126 Kasitsna Bay data sonde.

1127  
 1128  
 1129  
 1130  
 1131  
 1132  
 1133  
 1134  
 1135

1136 **Figure 6.**  
1137

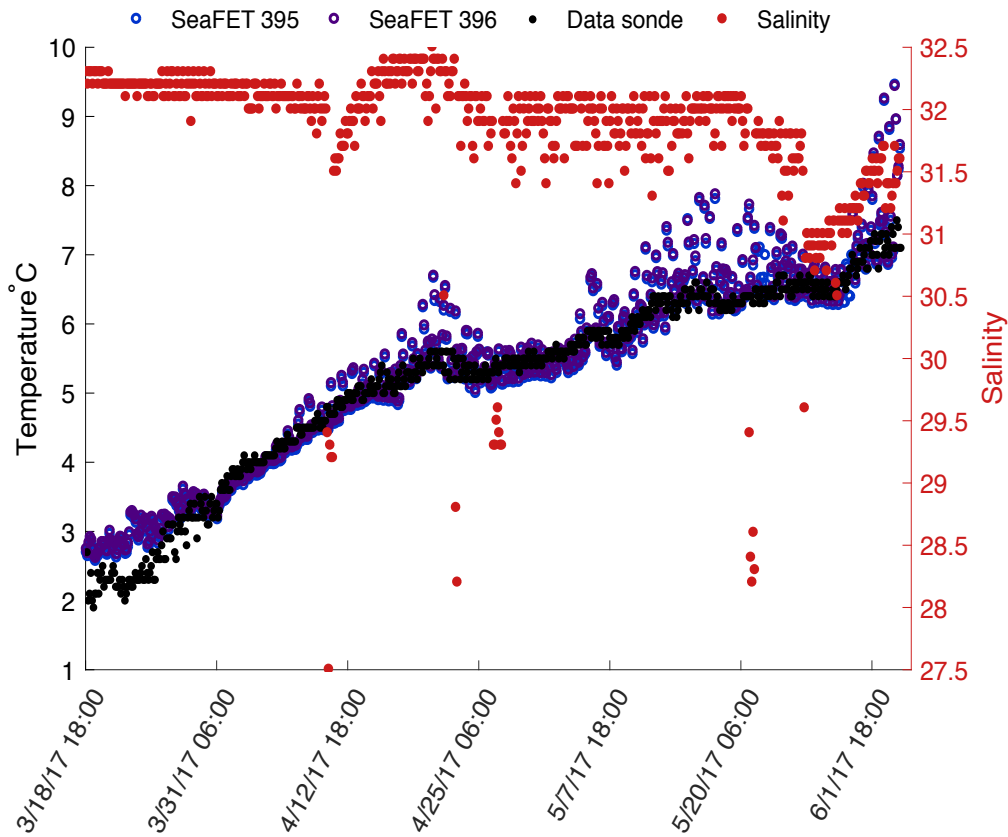


1138  
1139

1140 Mean  $pH_t$  anomaly between *in situ* single-point calibrated SeaFET<sup>TM</sup><sub>395</sub> and SeaFET<sup>TM</sup><sub>396</sub>  
1141 internal (panel a) and external (panel b) electrodes during parallel deployment in Kasitsna Bay,  
1142 AK. Intra-anomaly comparison based on calibration sample taken at initial deployment (< 24 h  
1143 non-conditioned, gray squares) and end of deployment (36 h pre-recovery, black squares).  
1144 Shaded blue region indicates conditioning period. Data points in blue region omitted when mean  
1145 anomaly was calculated (non-conditioned: transparent blue-dashed line; conditioned: bold blue-  
1146 dashed line) compared to mean anomaly from entire data set (non-conditioned to environment:  
1147 red-dashed line; conditioned: red-dashed line).

1148  
1149  
1150  
1151  
1152  
1153  
1154  
1155  
1156  
1157  
1158  
1159

1160 Figure 7.  
1161

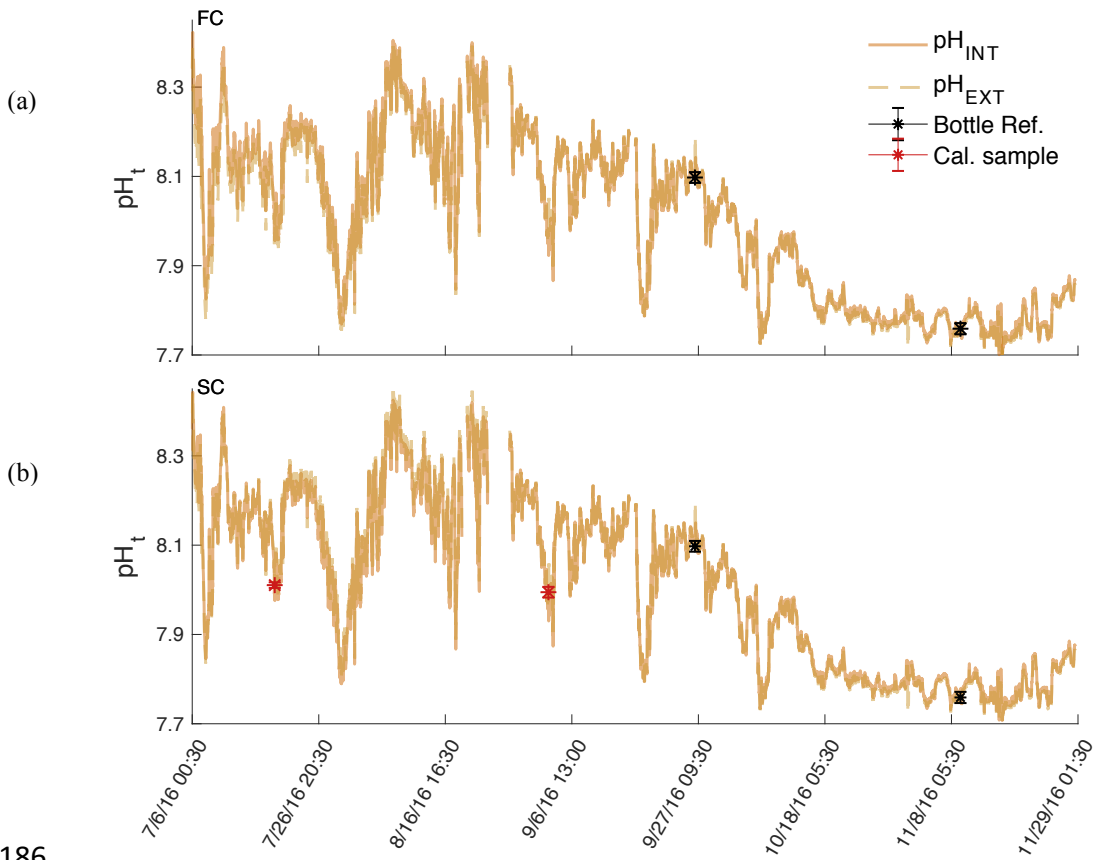


1162  
1163

1164 Temperature derived from the internal thermistor on SeaFET<sup>TM</sup><sub>395</sub> (blue) and SeaFET<sup>TM</sup><sub>396</sub>  
1165 (purple) compared against the temperature recorded by the Kachemak Bay National Estuarine  
1166 Research Reserve data sonde. Salinity (Red circles) recorded by Kachemak Bay data sonde on  
1167 the right y-axis.

1168  
1169  
1170  
1171  
1172  
1173  
1174  
1175  
1176  
1177  
1178  
1179  
1180  
1181  
1182  
1183

1184 **Figure 8.**  
1185



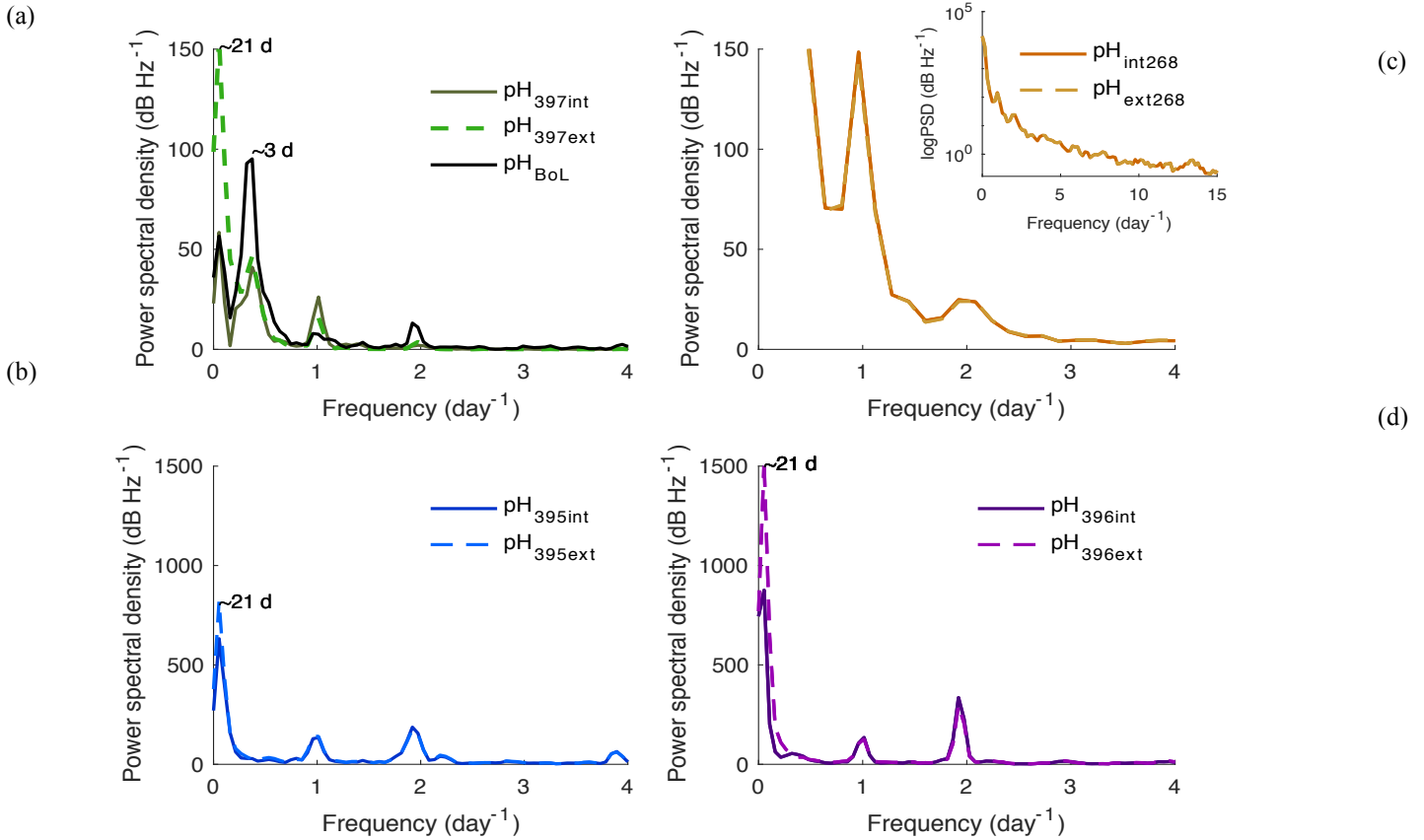
1186

1187  
1188  $pH_t$  recorded by the internal (solid) and external (dashed) electrodes on SeaFET<sup>TM</sup><sub>268</sub> deployed at  
1189 the Sentry Shoal mooring.  $pH_t$  from both electrodes is shown when derived using factory  
1190 calibration (FC) coefficients (panel a) and *in situ* single-point (SC) calibration coefficients (panel  
1191 b). Black asterisks are references samples taken after initial calibration and recalibration (red  
1192 asterisk), where  $pH_t$  was derived from  $TCO_2$  and  $pCO_2$  measurements made on the BoL at the  
1193 Hakai Institute's Quadra Island Field Station.

1194  
1195  
1196  
1197  
1198  
1199  
1200  
1201  
1202  
1203  
1204  
1205  
1206  
1207



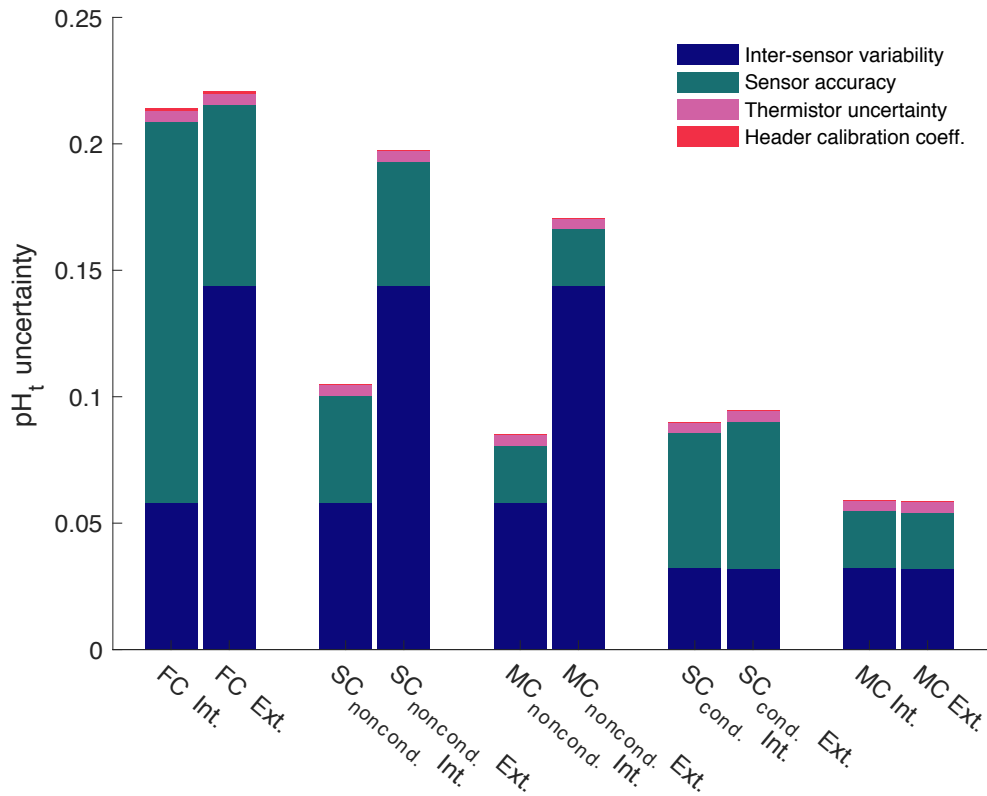
1208 **Figure 9.**  
 1209



1210  
 1211  
 1212  
 1213  
 1214  
 1215  
 1216  
 1217  
 1218  
 1219  
 1220  
 1221  
 1222  
 1223  
 1224  
 1225  
 1226  
 1227  
 1228  
 1229  
 1230

Power spectral density (PSD) analysis of  $\text{pH}_t$  in frequency per day for SeaFETs<sup>TM</sup> 397 (panel a), 268 (panel b), 395 (panel c), and 396 (panel c). Inset in panel b is log base 10 transformed PSD analysis of same data set. All internal electrodes marked as solid colored lines while external electrodes are colored dashed lines. BoL data set marked as solid black line (panel a).

1231 **Figure 10**  
 1232



1233  
 1234  
 1235 Quantified uncertainties based on field deployments of all Sea-Bird SeaFETs™ separated by  
 1236 electrode calibration method (FC: factory; SC: single-point; MC: multi-point), and calibration  
 1237 time for SeaFETs™ 395 and 396 (i.e., non-conditioned to environment and conditioned). pH<sub>t</sub>  
 1238 accuracy uncertainty calculated as the mean difference when comparing the absolute difference  
 1239 between reference samples and SeaFETs™ 395 (non-conditioned to environment and  
 1240 conditioned), 396 (non-conditioned to environment and conditioned), and 268 as well as the  
 1241 average absolute difference between SeaFET™ 397 and the BoL. Inter-sensor variability  
 1242 uncertainty determined by comparing SeaFETs™ 395 (non-conditioned to environment and  
 1243 conditioned) and 396 (non-conditioned to environment and conditioned), deployed side-by-side  
 1244 in Kasitsna Bay. Thermistor uncertainty is calculated pH<sub>t</sub> error when using thermistor derived  
 1245 temperature rather than external temperature sensor determined from SeaFETs™ 395 and 396.  
 1246 Header calibration coefficient uncertainty is the discrepancy in pH<sub>t</sub> when using SeaFETcom  
 1247 factory calibration coefficients from header file rather than disc file.  
 1248  
 1249